PEOPLE'S DEMOCRATIC REPUBLIC OF ALGERIA

MINISTRY OF HIGHER EDUCATION AND SCIENTIFIC RESEARCH

UNIVERSITY OF MOHAMED BOUDIAF-M'SILA-

COLLEGE OF TECHNOLOGY

ELECTRONICS DEPARTMENT

N :……

SECTOR: SCIENCE AND TECHNOLOGY

SPECIALTY: ELECTRONICS

OPTION: INSTRUMENTATION

A THESIS SUBMITTED FOR THE DEGREE OF: MASTER

THEME:

Trimodal Generalized Gamma Distribution of Sea Echoes and CFAR Detection in CG-LNT Clutter with Multiple Order Statistics

Presented by

DJEMAI Boutheyna

Supported 18/06/2025

Supported by a jury of:

Dr. Mezaache Hatem	President	Departement of Electronics
Pr. Mezache Amar	Supervisor	Departement of Electronics
Pr. Oudira Houcine	Co-Supervisor	Departement of Electronics
Pr. Benahcen Madani	Examiner	Departement of Electronics

Academic year : 2024 / 2025

Abstract

In this thesis, a comprehensive study of radar systems and their basic concepts are presented firstly. Next, the problem of interference faced by radars and its impact on detection accuracy is also evoked. Then, radar clutter types and targets fluctuating models are also highlighted. Research works concerned in this thesis deal with the improvements of high resolution sea clutter modeling and CFAR detection in presence of interfering targets.

The first research problem focuses on the use of mixture generalized gamma (GG) distribution named Trimodal GG distribution in order to provide an accurate model that reflects the description characteristics of the majority of sea clutter scenarios. Comparison purposes are conducted against GG, mixture of two GG, *K*+noise and CG-LNT+noise (Compound Gaussian Log-Normal Texture) models. Parameters estimation is obtained by the well known LSA (Least Squares Approximation) approach. The modeling results show that the proposed Trimodal GG model is able to fit most scenes of IPIX (Intelligent PIxel X-band radar) real data.

The second research problem is to enhance CFAR (Constant False Alarm Rate) properties in presence of homogeneous and heterogeneous CG-LNT sea clutter. To achieve this, existing WHWH (Weber Haykin-Weber Haykin))-CFAR and OS (Order Statistic)-CFAR algorithms are combined by means of a general test statistic. This detector is labeled WHWHOS-CFAR and is compared with available logt-, OS-, WH-, WHOS- and WHWH-CFAR detectors. Through, simulated and IPIX real data, it is shown that the proposed WHWHOS-CFAR detector exhibits the best CFAR properties and provides a worst CFAR loss only for a special value of the standard deviation clutter parameter.

Key words: Sea clutter, Trimodal GG model, CFAR detection, CG-LNT distribution, WHWHOS-CFAR detector.

Résumé

Dans cette thèse, une étude approfondie des systèmes radar et leurs concepts de base sont présentées. Le problème des interférences rencontrées par les radars et son impact sur la précision de la détection des cibles est également évoqué. Les types de clutter radar et les modèles de cibles fluctuantes sont mis en évidence. Les travaux de recherche concernés par cette thèse portent sur l'amélioration de la modélisation de clutter marin à haute résolution ainsi que la détection CFAR en présence de cibles interférentes.

Le premier problème de recherche porte sur l'utilisation de la distribution gamma généralisée (GG) mélangée appelée distribution Trimodal GG afin d'obtenir un modèle précis qui reflète les caractéristiques de description de la majorité des scénarios de clutter de la mer. Les de comparaisons sont menées avec les modèles GG, mélange de deux modèles GG, K+noise et CG-LNT+noise (Compound Gaussian Log-Normal Texture). L'estimation des paramètres est obtenue par la méthode LSA (Least Squares Approximation). Les résultats de la modélisation montrent que le modèle Trimodal GG proposé est capable d'adapter la plupart des scènes de données réelles IPIX (Intelligent PIxel X-band radar).

Le deuxième problème de recherche est d'améliorer les propriétés CFAR (Constant False Alarm Rate) en présence du clutter marin CG-LNT distribué homogène et hétérogène. Pour ce faire, les algorithmes WHWH (Weber Haykin-Weber Haykin))-CFAR et OS (Order Statistic)-CFAR sont combinés au moyen d'une statistique de test générale. Ce détecteur est appelé WHWHOS-CFAR et il est comparé devant les détecteurs existants logt, OS, WH, WHOS et WHWH-CFAR. Utilisant les données simulées et réelles IPIX, il est montré que le détecteur WHWHOS-CFAR proposé présente des meilleures propriétés CFAR et fournit une perte CFAR mais pour une seule valeur du paramètre d'écart-type de clutter.

Mot clés : Clutter de la mer, Distribution Trimodal GG, Détection CFAR, Distribution CG-LNT, Détecteur WHWHOS-CFAR.

ملخص

تقدم هذه الأطروحة دراسة شاملة لأنظمة الرادار ومفاهيمها الأساسية. كما تمت مناقشة مشكلة التداخل الذي يواجهه الرادار وتأثيره على دقة اكتشاف الهدف. سيتم تسليط الضوء على أنواع فوضى الرادار ونماذج الأهداف المتقلبة. يركز العمل البحثي المعني في هذه الأطروحة على تحسين نمذجة الفوضى البحرية عالية الدقة بالإضافة إلى اكتشاف CFAR في وجود أهداف متداخلة.

تتعلق مشكلة البحث الأولى باستخدام توزيع جاما المعمم المختلط (GG) المسمى Trimodal GG للحصول على نموذج دقيق يعكس خصائص الوصف لمعظم سيناريوهات الفوضى البحرية. يتم إجراء المقارنات مع نماذج GG، و مزيج من نموذجين GG، K+noise وCG-LNT+noise (نسيج لوغاريتمي غاوسي مركب طبيعي). يتم الحصول على تقدير الثوابت بواسطة LSA (تقريب المربعات الصغرى). تظهر نتائج النمذجة أن نموذج Trimodal GG المقترح قادر على تكييف معظم مشاهد البيانات الحقيقية IPIX (رادار النطاق X الذكي PIxel).

تتمثل مشكلة البحث الثانية في تحسين خصائص CFAR (معدل الإنذارالخاطئ الثابت) في وجود فوضى بحرية موزعة متجانسة وغير متجانسة CG-LNT. للقيام بذلك، يتم الجمع بين خوارزميات CFAR-((Weber Haykin-Weber Haykin) WHWH وOS (إحصاء الترتيب)-CFAR باستخدام إحصاء اختبار عام. يُطلق على هذا الكاشف اسم WHWHOS-CFAR ويتم مقارنته بكاشفات logt وOS وWH وWHOS وWHWH-CFAR الموجودة. وباستخدام بيانات IPIX المحاكاة والحقيقية، تبين أن الكاشف WHWHOS-CFAR المقترح يتمتع بخصائص CFAR أفضل ويوفر خسارة CFAR ولكن لقيمة واحدة فقط من معامل الانحراف المعياري للفوضى.

كلمات المفتاح: فوضى البحر، توزيع GG ثلاثي الوسائط، كشف CFAR، توزيع CG-LNT و الكاشف WHWHOS-CFAR.

Acknowledgements

*I thank **ALLAH Almighty** for giving me the strength, patience, and will to complete this work.*

*I would like to thank **Pr. Amar Mezache**, who agreed to supervise me. I particularly thank him for allowing me to benefit from his scientific skills, human qualities, and constant presence. I also thank **Pr. Houcine Oudira**, who also supervised and assisted in the completion of this work.*

*I would also like to thank **the members of the jury** who agreed to judge this research work.*

Finally, I extend my sincere gratitude to all those who, through their support and encouragement, made this work possible.

Dedicate

To my dear parents: Ali and Akila.

To my brother: Abde Lwahhab.

To my sisters: Mounira, Hanane, Rachida, and Khalissa.

To all my family and friends.

Boutheyna

Contents

Abstract ……..……..….i

Résumé ……..……ii

ملخص iii

Acknowledgements ……..…….…iv

Dedicate ……..…….....…….....v

Contents ……..vi

List of Figures ……..……..…….…..viii

List of Tables …….…….....xi

List of Abbreviations ……..……...xii

List of Nomenclature ……..……..xiv

General Introduction ……...……..1

1. Introduction ……...…….…...1

2. Thesis works ……..……2

3. Thesis Organization ……..……..…..3

Chapter 1: Radar System Overview…….4

1.1 Introduction ……...……....……..……5

1.2 History of systems radar ……...…….…..…….....…5

1.3 Basic elements of a radar system ……..……..…...6

1.4 Principle of operation of radar system ……..…….……...…8

1.5 Radar system equations ……..…….…….....9

1.6 Radar systems classification ……...…….……12

1.7 Applications of radar system ……...14

1.8 Radar clutter ……...……15

1.9 Radar targets ……..……...……18

1.10 False alarm probability ……..……....19

1.11 Conclusion ……..…….....…..…..……21

Chapter 2: Modeling of High-Resolution Sea-Clutter ……..…….…..……22

2.1 Introduction …….……..……23

2.2 Sea-Clutter Distributions …….……..……..…..23

2.3 Mixture GG Clutter model ……..…….…….26

2.4 Parameter Estimation …….……..…….27

2.5 Experimental Results ……..…….…….…29

2.6 Conclusion …….…….……..…..37

Chapter 3: CFAR Detection in CG-LNT Clutter and Multiple Targets Situations.……..…….……38

3.1 Introduction ……..……..……..…..…39

3.2 WHWHOS-CFAR Detector ……..…….…… …..39

3.3 Detection Performance Comparisons …….……...41

3.4 Conclusion ……...……..……...…...56

General Conclusion ……..……..……...…57

References ….……...…59

List of Figures

Figure 1.1 The principle of radar operation in detecting targets using electromagnetic waves ……...…… **9**

Figure 1. 2 Radar system classification …… **12**

Figure 1. 3 Envelop detector of radar echoes with an intermediate Envelop detector of radar echoes with an intermediate.…… **16**

Figure 1. 4 Definition of a resolution volume…….. **16**

Figure 1. 5 Radar echoes from the sea surface (i.e., radar footprint) Radar echoes from the sea surface (i.e., radar footprint) ……..... **18**

Figure 1. 6 A typical radar ROC graph …… **21**

Figure 2. 1 Flowchart of the simplex minimization algorithm of (2.24) ……. **29**

Figure 2. 2 Modeling of IPIX real data for HH polarization, 9th range cell and 3m resolution..... **33**

Figure 2. 3 Modeling of IPIX real data for HH polarization, 17th range cell and 3m resolution. …….. **33**

Figure 2. 4 Modeling of IPIX real data for HH polarization, 30th range cell and 3m resolution……. **34**

Figure 2. 5 Modeling of IPIX real data for VV polarization, 12th range cell and 3m resolution.…… **34**

Figure 2. 6 Modeling of IPIX real data for HH polarization, 3rd range cell and 15m resolution……. **35**

Figure 2. 7 Modeling of IPIX real data for VV polarization, 15th range cell and 15m resolution.…… **35**

Figure 2. 8 Modeling of IPIX real data for HH polarization, 4th range cell and 30m resolution.……... **36**

Figure 2. 9 Modeling of IPIX real data for VV polarization, 22th range cell and 30m resolution.……... **36**

Figure 3. 1 Existing CFAR detectors in CG-LNT clutter with known σ…… **40**

Figure 3. 2 Illustration of CFAR property of logt-CFAR detector in CG-LNT sea-clutter with M = 32 and $\delta = \exp(\sigma^2 / 2)^{-1}$…….. **44**

Figure 3. 3 Illustration of CFAR property of logt-CFAR detector in CG-LNT sea-clutter with M = 32 and $\delta = \exp(\sigma^2 / 2)^{-1}$…….. **44**
Figure 3. 4 Illustration of CFAR property of WH-CFAR detector in CG-LNT sea-clutter with M = 32 and $\delta = \exp(\sigma^2 / 2)^{-1}$. ……. **45**
Figure 3. 5 Illustration of CFAR property of WHOS-CFAR detector in CG-LNT sea-clutter with M = 32 and $\delta = \exp(\sigma^2 / 2)^{-1}$…… **45**
Figure 3. 6 Illustration of CFAR property of WHWH-CFAR detector in CG-LNT sea-clutter with M = 32 and $\delta = \exp(\sigma^2 / 2)^{-1}$. …… **46**
Figure 3. 7 Illustration of CFAR property of WHWHOS-CFAR detector in CG-LNT sea-clutter with M = 32 and $\delta = \exp(\sigma^2 / 2)^{-1}$……. **46**
Figure 3. 8 CFAR properties study of different CFAR detectors in terms of σ with M = 32 and $\delta = \exp(\sigma^2 / 2)^{-1}$. …….. **47**
Figure 3. 9 CFAR properties study of different CFAR detectors in terms of σ with 1 interfering target (ICR = 10 dB), M = 32 and $\delta = \exp(\sigma^2 / 2)^{-1}$. …….. **47**
Figure 3. 10 CFAR properties study of different CFAR detectors in terms of σ with 2 interfering target (ICR = 10 dB), M = 32 and $\delta = \exp(\sigma^2 / 2)^{-1}$…… **48**
Figure 3. 11 CFAR property of logt-CFAR detector in CG-LNT sea-clutter using real IPIX data……..... **48**
Figure 3. 12 CFAR property of OS-CFAR-CFAR detector in CG-LNT sea-clutter using real IPIX data.…… **49**
Figure 3. 13 CFAR property of WH-CFAR-CFAR detector in CG-LNT sea-clutter using real IPIX data ……..... **49**
Figure 3. 14 CFAR property of WHOS-CFAR-CFAR detector in CG-LNT sea-clutter Using real IPIX data……. **50**
Figure 3. 15 CFAR property of WHWH-CFAR-CFAR detector in CG-LNT sea-clutter using real IPIX data.……. **50**
Figure 3. 16 CFAR property of WHWHOS-CFAR-CFAR detector in CG-LNT sea-clutter using real IPIX data.……. **51**
Figure 3. 17 CFAR properties study of different CFAR detectors in terms of σ, M = 32 and $\delta = \exp(\sigma^2 / 2)^{-1}$…… **51**
Figure 3. 18 Detection probability of CFAR algorithms as a function of SCR for M = 32, σ = 0.5 and $\delta = \exp(\sigma^2 / 2)^{-1}$…… **52**

Figure 3. 19 Detection probability of CFAR algorithms as a function of SCR for M = 32, σ = 1.5 and δ = exp (σ^2 / 2) $^{-1}$. ……. **53**

Figure 3. 20 Detection probability of CFAR algorithms as a function of SCR for 1 interfering target, M = 32, σ =0.5 and δ = exp (σ^2 / 2) $^{-1}$……... **53**

Figure 3. 21 Detection probability of CFAR algorithms as a function of SCR for 1 interfering target, M = 32, σ =1.5 and δ = exp (σ^2 / 2) $^{-1}$ …….. **54**

Figure 3. 22 Detection probability of CFAR algorithms as a function of SCR using real data for M = 32, HH polarization and resolution 3m…….. **54**

Figure. 3. 23 Detection probability of CFAR algorithms as a function of SCR using real data for 1 interfering target, *M* = 32, HH polarization and resolution 3m …….. **55**

Figure. 3. 24 Detection probability of CFAR algorithms as a function of SCR using real data for 2 interfering target, *M* = 32, HH polarization and resolution 3m ……... **55**

List of Tables

Table 1. 1 Application areas of radar systems …….……. 15

Table 2. 1 Properties of IPIX recorded data collected at Grimsby, Ontario, Canada ……... 31

Table 3. 1 Possible CFAR test statistics obtained from …… 41

Table 3. 2 Corresponding, parameters values found for each CFAR detector for **M=32** …. 42

Liste of Abreviations

RADAR	RAdio Detection And Ranging
CFAR	Constant False Alarm Rate
CG	Compound-Gaussian
CG-LNT	Compound Gaussian Log-Normal Texture
IPIX	Intelligent PIxel X-band
IF	Intermediate Frequency
STC	Sensitivity Time Control
ADC	Analog-to-Digital Converter
PSR	Primary Surveillance Radar
CW	Continuous Wave
ASR	Airport Surveillance Radar
ASDE	Airport Surface Detection Equipment
ARSR	Air Route Surveillance Radars
RCS	Radar Cross Section
SNR	Signal to Noise Ratio
ROC	Receiver Operating Characteristics
MLE	Maximum Likelihood Estimator
GG	Generalized Gamma
CNR	Clutter-to-Noise Ratio
PDF	Probability Density Function

CCDF	Complementary CDF
CRP	Clutter Range Profile
SM	Simplex Minimization
CDF	Cumulative Distributed Function
RCP	Range Clutter Profile
RF	Radio Frequency
SCR	Signal-to-Clutter Ratio
H_0	Null hypothesis
H_1	Alternate hypothesis
iid	independent and identically distributed
OS-CFAR	Order-Statistics-CFAR
WH-CFAR	Weber-Haykin-CFAR
CUT	Cell Under Test
PFA	False Alarm Probability
Pd	Detection Probability

List of Nomenclature

$\widetilde{\boldsymbol{A}}$	Received amplitude.
$\widetilde{\boldsymbol{\varphi}}$	Received phase.
Q	Quadrature component.
I	In phase component.
R	Radar range.
c	Light speed.
τ	Sampling period.
σ^2	Variance.
S_{min}	Minimum detectable signal power.
R_{max}	Maximum radar range.
c	A Clutter area.
$\boldsymbol{\psi_g}$	Grazing angle.
c	Scale parameter of the K-distribution.
ν	Shape parameter of the K-distribution.
α	Shape parameter of the Pareto type II distribution.
β	Scale parameter of the Pareto type II distribution.
a	Scale parameter of the GC distribution.
$V_{1.2}$	Shape parameters of the GC distribution.
Z	Observation space.
μ	Median.
P_{FA}	False alarm probability.
P_D	Detection probability.
P_M	Miss Probability
$p(H_0)$, $p(H_1)$	Priori probabilities.
T	Detection threshold.
P_n	Noise power.
$\Gamma(.)$	Gamma function.
ln(x)	Log of the random variable

$\hat{\mu}$	Estimated mean
$\hat{\boldsymbol{\sigma}}$	Estimated standard deviation of the random variable log(X).
N	CRP size.
$\boldsymbol{\alpha}$	Shape parameter.
θ	Beam width.
β	the scale parameter
γ (.,.)	Lower incomplete gamma function.
E	Electric field.
H	Magnetic field.
r^{th}	Raw moment
$\boldsymbol{\varphi}$	Psi (digamma) function
$\langle . \rangle$	Empirical mean
$\boldsymbol{\tau}$	Scale factor

General Introduction

1. Introduction

The history of radar (**RA**dar **D**etection **A**nd **R**anging) systems is a long and complex narrative, representing the culmination of research conducted by scientists from various countries. Radar experienced significant growth during World War II, with notable technological advancements occurring in several countries such as the United States, Germany, and the United Kingdom. After the 2nd world war, its applications expanded into civilian domains, particularly in aviation for air traffic control, as well as in diverse fields like meteorology and archaeology [1].

Due to the intricate physical mechanisms of sea clutter, its amplitude distribution exhibits highly variable tails under different radar and environmental conditions. However, existing statistical models such as Rayleigh, Weibull, log-normal, etc have limited ability to capture such variability. This limitation impedes a comprehensive understanding of clutter characteristics and can result in mismatches between real-world data and the selected clutter models, potentially degrading radar performance in model-based applications such as clutter classification, target detection, and tracking [2].

Target detection in sea clutter has attracted ample attention in detection theory. It is also one of the most complicated problems in radar signal processing. Sea clutter exhibits strong non-stationary along time and range cells, which interferes gravely target detection, low-velocity weak targets in particular. Low-velocity small target detection in sea has not only been widely applied in military affairs and maritime rescue, but also considered to be a hot-point problem in radar signal processing [3].

2. Thesis works

Based on the above discussions, two research issues in radar signal processing are considered in this work; modeling of sea clutter and CFAR (Constant False Alarm Rate) detection in sea clutter.

2. 1 Modeling of Sea Clutter

In order to obtain an accurate fit with sea reverberation data, we propose, in this thesis, a Trimodal GG (generalized gamma) disturbance model. The LSA (Least Squares Approximation) approach is used to avoid computational complexities associated with the MLE (maximum likelihood estimator) and moments-based estimators. Metric tests against recorded real life IPIX (Intelligent PIxel X-band radar) database are worked out to assess the proposed and standard CG-LNT, GG, CG-LNT+noise, K+noise and mixture GG distributions. It is show that the Trimodal GG distribution is validated to be in qualitative agreement with different cell resolutions of available IPIX database.

2. 2 CFAR Detection in Sea Clutter

The problem of targets CFAR detection embedded in homogeneous and heterogeneous CG-LNT (compound Gaussian log-normal texture) distributed clutter is addressed in this thesis. The latter is expressed in terms of two parameters; standard deviation parameter and scale parameter. It possesses a strong ability to model various sea clutter scenarios. Based on the general test statistic, two non-negatives invariants functions were selected and the proposed WHWHOS-CFAR was derived. The detection performances of logt-, OS- (Order Statistic), WH-(Weber Haykin), WHOS-, WHWH- and the proposed WHWHOS-CFAR algorithms are examined for Swerling 1 target type. In the presence of interfering targets, OS-, WH-, WHOS- WHWH- and WHWHOS-CFAR CFAR detectors are considered where the CFAR properties are investigated as a function of clutter parameters.

3. Thesis Organization

The manuscript is organized as follows:

Chapter 1 introduces some necessary concepts to understand about radar systems and their crucial role in various domains. Then, it discusses types of radar echoes as well as volume clutter, surface clutter and fluctuating targets returns. Some definitions about false alarm and detection probabilities are also presented at the end of this Chapter.

Chapter 2 outlines the three-parameter GG distribution and recalls some standards statistical distributions that will be used for comparison purposes. Then, the mixture GG with two and three GG distributions are considered for IPIX real data modeling by means of the NLSA estimation method of their parameters. Next, fitting of several IPIX real data scenes using proposed and conventional distributions are studied.

Chapter 3 highlights the operation of standard and proposed WHWHOS-CFAR detectors operating in homogeneous and heterogeneous background. Comparison purposes of CFAR properties and detection probabilities of the different CFAR procedures are then presented and commented.

Finally, main conclusions are inspired from simulated and experimental results obtained in this work including modeling of sea clutter and CFAR detection of Swerling 1 targets in CG-LNT distributed clutter.

Chapter 1

Radar System Overview

Abstract:

This Chapter covers the general concepts of radar systems, starting with their definition and history. It then covers the operating principle, basic components, equations, classification, and applications. Radar clutter, radar targets, and the possibility of false alarms and detection are also addressed.

Chapter outline:

1. 1 Introduction……..…….5
1. 2 History of Systems Radar……..…….....…5
1. 3 Basic Elements of a Radar System…….....6
1. 4 Principle of Operation of Radar System…….…….…..…8
1. 5 Radar System Equations……..…….……..….....9
1. 6 Radar Systems Classification…….……..12
1. 7 Applications of Radar System……..…....14
1. 8 Radar Clutter ……..…….....15
1. 9 Radar Targets …….……..18
1. 10 False Alarm Probability ……..……..….....19
1. 11 Conclusion ...……..…….....…..…..…21

1. 1 Introduction

The term radar, short for "**RA**dio **D**etection **A**nd **R**anging," is a system that operates using electromagnetic waves. Initially, its primary function was detection. Over time, radar has undergone significant development thanks to research that has enabled it to perform many other functions. It is particularly used in certain fields, such as military, aviation, marine, meteorology, and road safety [1]. In the rest of this Chapter, we will introduce some of the basic concepts necessary to understand about radar systems.

This Chapter aims to provide a comprehensive understanding of radar systems and their crucial role in various domains.

1. 2 History of Systems Radar

The history of radar systems is a long and complex narrative, representing the culmination of research conducted by scientists from various countries. Here's an overview of the key milestones in the development of radar.

1. 2. 1Theoretical Foundations:

1865: English physicist James Clerk Maxwell developed his theory of electromagnetic light, laying the groundwork for understanding how electromagnetic waves propagate.

1886: German physicist Heinrich Rudolf Hertz demonstrated the physical existence of electromagnetic waves, thereby confirming Maxwell's theory.

1. 2. 2Early Inventions:

1904: German technician Christian Hülsmeyer invented the "Telemobiloskop", a device aimed at preventing maritime collisions. This device measured the time it took for an electromagnetic wave to travel to and from a metallic object (such as a ship), allowing for distance calculation. Hülsmeyer patented his invention in Germany, France, and the United Kingdom.

1921: Albert Wallace Hull developed a high-efficiency oscillator known as the magnetron, which would later become crucial for radar systems.

1922: Albert. H. Taylor and Leo C. Young, from the Naval Research Laboratory (USA) detected a wooden ship for the first time using a method similar to that of Hülsmeyer.

1930: Lawrence A. Hyland, also from the Naval Research Laboratory, achieved the first detection of an aircraft.

1. 2. 3 The Rise of Modern Radar:

1934: Systematic tests on shortwave detection systems were conducted in France, leading to a patent being filed. The cargo ship Oregon was the first to be equipped with radar.

1935: Robert Watson-Watt filed a patent for a British radar network known as Chain Home, which became operational.

1936: The klystron was developed by Metcalf and Hahn, serving as an amplifier in radar systems.

1940: Various Radar equipments are developed in the USA, Russia, Germany, France and Japan [1].

Radar experienced significant growth during World War II, with notable technological advancements occurring in several countries such as the United States, Germany, and the United Kingdom. After the war, its applications expanded into civilian domains, particularly in aviation for air traffic control, as well as in diverse fields like meteorology and archaeology.

1. 3 Basic Elements of a Radar System

A radar system consists of several basic components including a signal generator that generates high-frequency electromagnetic signals, a radar antenna that directs these signals into the space to be explored, a radar receiver that receives signals reflected from targets, and a processing system that analyzes the signals to extract useful information such as the target's location, speed, and direction. The radar mechanism depends on sending and receiving signals after they are reflected from targets, which allows the distance and direction to be determined using the round-trip time of the signals.

1. 3. 1 Transmitter: The transmitter converts mains power into radio frequency power, which leaves the radar by the antenna to illuminate its surroundings in the same way as a searchlight. The waveguide or transmission line system connects the transmitters and receivers to a common antenna.

1. 3. 2 Antenna: The antenna directs the transmitter energy into a beam that illuminates the radar's surroundings. The echoes of the illumination are gathered by the

antenna for the receivers. The antenna is the principal filter to attenuate signals (interference or jamming) coming from other directions. Once the radio frequency energy leaves the antenna, it is subject to atmospheric refraction and attenuation.

1. 3. 3 Receiver: The receiver is normally a super heterodyne receiver with one or more intermediate frequencies. The first stage of the receiver is the principal component that defines the noise level and thus the sensitivity of the radar. The signals that arrive at the signal processor must not be distorted so they may be separated into the original components without the distortion components. The use of sensitivity time control (STC) reduces the necessity for a very wide dynamic in the receiver circuits. The matched filter has a shape and a bandwidth that gives best selection of signal energy out of the mixture of signals and noise coming from the receiver. These filters are often difficult to produce, so commonly simpler filters are used, called matching filters.

1. 3. 4 Detector: The intermediate frequency signals need to be detected before they can be displayed. Simpler detectors reject either phase or amplitude information, and change the statistics of the thermal noise on a theoretical carrier from the receiver. Coherent signal processors, which follow detectors, require the full amplitude and phase information in the echo signals. This information is preserved in vector detectors. The most common detector circuit is a synchronous detector that offers the in-phase (*I*) component and the quadrature (*Q*) phase component of the received vector.

1. 3. 5 Analogue-to-digital converter: Digital signal processors perform arithmetic on trains of binary numbers that represent the signals. Analogue to digital converters convert the signals, normally from a vector detector, to digital form. The side effects are the limiting of the dynamic range, quantization noise, and distortion. Even in more modern systems in which the signal is sampled at the intermediate frequency (IF) with a single analog-to-digital converter (ADC), an algorithm implemented in the system firmware constructs the *I* and *Q* components of the signal for processing the envelop,

$$\boldsymbol{V = \sqrt{I^2 + Q^2}} \tag{1.1}$$

1. 3. 6 Signal processor: Signal processing may take place during one sweep, many sweeps, and many scans. Radar echoes are a mixture of wanted echoes (for example, aircraft) and clutter echoes (often from land, sea, weather, or birds), which are generally of no interest. Signal processing tries to filter the echoes for the user and match them to his display. Modern digital processing often causes the echoes to be displayed as synthetic shapes that show only the information for which it has been preprogrammed. In contrast, radar operators who use

older equipment are used to identifying echoes by size, shape, and movement. The evaluation of these criteria takes time and greatly reduces the number of echoes that an operator may follow, but it may be critical in unusual or unforeseen situations.

1. 3. 7 Detection and measurement results: After the signals have been filtered to exclude out-of-band noise, the pulse has been compressed (when necessary), and the clutter and interference have been reduced to the noise level, a decision is made as to whether the echo signal represents an object of interest. The decision may be made automatically or by an operator. Once the echo signals have been detected, the position, radial velocity and classification of the object must be estimated. The echo signals are combined with noise and the measurement accuracy depends on the signal-to-noise ratio (SNR) [4].

1. 4 Principle of Operation of Radar System

Radar uses a principle similar to the reflection of sound waves. When you emit sound in the direction of an object that can reflect your sound (such as a valley or cave), you hear an echo. If you know the speed of sound in the air, you can estimate the distance and general direction of the object. The time taken to reach and return can be converted into distance if you know the speed of sound.

Radar works similarly, sending out high-frequency electromagnetic energy signals. A small portion of the emitted wave "energy" is reflected back to the radar by the target; this signal is called a reflected wave "echo". The radar captures this echo with a time delay, $\boldsymbol{\tau}$, allowing it to determine the distance and possibly the speed of the target.

The distance, ***d,*** between the target and the radar can be calculated from the relationship:

$$\boldsymbol{d = \frac{C \times \tau}{2}} \tag{1.2}$$

C: is the speed of light ($C \approx 299{,}792{,}458\ m/s$).

$\boldsymbol{\tau}$: is the time it takes the pulse to travel back and forward [5].

The radar system consists of a powerful transmitter that sends signals through a multiplexer that directs them to an antenna. Each target reflects the signal in multiple directions, a process called "dispersion". The portion of the signal returned in the direction of the radar is called "back reflection". The echo from the target is directed to the radar antenna by the multiplexer to a highly sensitive receiver. As shown in the Figure 1.1.

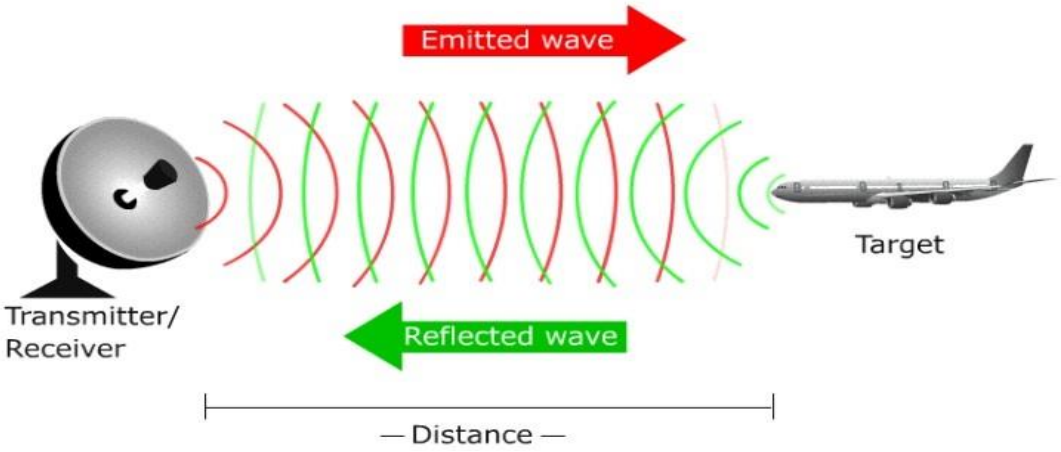

Figure 1.1 The principle of radar operation in detecting targets using electromagnetic waves.

1. 5 Radar System Equations

The radar range equation (or radar equation, for short) not only serves the very useful purpose of estimating the range of radar as a function of the radar characteristics, but also is quite useful as a guide for designing a radar system. The simple form of the radar equation may be written as

$$P_r = \frac{P_t G_t}{4\pi R^2} \times \frac{\sigma}{4\pi R^2} \times A_e \tag{1.3}$$

The right-hand side has been written as the product of three factors to represent the physical processes that take place. The first factor on the right is the power density at a distance R from radar that radiates a power P_t, from an antenna of gain G_t. The numerator σ of the second factor is the radar cross section of the target. It has the unit of area (for example, square meters) and is a measure of the energy redirected by the target back in the direction of the radar. The denominator of the second factor accounts for the divergence of the echo signal on its return path back to the radar. The product of the first two factors represents the power per unit area returned to the radar antenna. Note that the radar cross section of target, σ is defined by this equation. The receiving antenna of effective area, A_e, collects a portion P_t, of the echo power returned to the radat. If the maximum radar range, R_{max} is defined as

occurring when the received signal is equal to the minimum detectable signal of the radar, S_{min} the simple form of the radar equation becomes

$$R_{max}^4 = \frac{P_t G_t A_e \sigma}{(4\pi)^2 S_{min}} \tag{1.4}$$

Generally, most radars use the same antenna for both transmitting and receiving. From antenna theory, there is a relation between the gain, G_t, of the antenna on transmit and its effective area A_e, on receive, which is, $G_t = 4\pi A_e/\lambda^2$ where λ is the wavelength of the radar signal. Substituting this into (1.4) provides two other useful forms of the radar equation (not shown here) one that represents the antenna only by its gain and the other that represents the antenna only by its effective area.

The simple form of the radar equation is instructive, but not very useful since it leaves out many things. The minimum detectable signal S_{min} is limited by receiver noise and can be expressed as

$$S_{min} = kT_O B F_n (S/N)_1 \tag{1.5}$$

In this expression, kT_O is the so-called thermal noise from an ideal conductor, where k = Boltzmann's constant, T_O is the standard temperature of 290 K. and B = receiver bandwidth (usually that of the IF stage of the super-heterodyne receiver). The product kT_O is equal to $4 \times 10^{-21} W/Hz$. To account for the additional noise introduced by a practical (nonideal) receiver, the thermal nouse expression is multiplied by the noise figure F_n of the receiver, defined as the noise out of a practical receiver to the noise out of an ideal receiver. For a received signal to be detectable, it has to be larger than the receiver noise by a factor denoted here as signal-to-noise ratio SNR. This value of SNR, is that required if only one pulse is present. It has to be large enough to obtain the required probability of false alarm (due to noise crossing the receiver threshold) and the required probability of detection (as can be found in various radar texts) Radars, however, generally process more than one pulse before making a detection decision. We assume the radar waveform is a repetitive series of rectangular-like pulses. These pulses are integrated (added together) before a detection decision is made. To account for these added signals, the numerator of the radar equation is multiplied by a factor, $nE_i(n)$, where $E_i(n)$ is the efficiency in adding together *n* pulses. This value can also be found in standard texts.

The power P_t, is the peak power of a radar pulse. The average power, P_{av}, is a better measure of the ability of a radar to detect targets, so it is sometimes inserted into the radar equation using $P_t = P_{av}/f_P$, where f_P is the pulse repetition frequency of the pulse radar and τ is the pulse duration. The surface of the earth and the earth's atmosphere can drastically affect the propagation of electromagnetic waves and change the coverage and capabilities of radar. In the radar equation, these propagation effects are accounted for by a factor F^4 in the numerator of the radar equation. With the above substituted into the simple form of the radar equation we get

$$R_{max}^4 = \frac{P_{av} G A_e \sigma \, n E_i(n) F^4}{(4\pi)^2 \, k T_o F_n \, f_P (S/N)_1 L_s} \tag{1.6}$$

In the above equation, it was assumed in its derivation that $B\tau \approx 1$, which is generally applicable in radar. A factor, L_S, (greater than unity), called the system losses, has been inserted to account for the many ways that loss can occur in a radar. This loss factor can be quite large. If the system loss is ignored, it might result in a very large error in the estimated range predicted by the radar equation. A loss of from 10 dB to may be 20 dB is not unusual when all radar system loss factors are taken into account.

Equation (1.6) applies for a radar that observes a target long enough to receive *n* pulses. More fundamentally, it applies for a radar where the time on target t_O, is equal to n/f_P. An example is a tracking radar that continuously observes a single target for a time t_OThis equation, however, needs to be modified for a surveillance radar that observes an angular volume Ω with a revisit time, t_S. (Air traffic control radars might have a revisit time of from 4 to 12 s.) Thus, a surveillance radar has the additional constraint that it must cover an angular volume Ω in a given time, t_S. The revisit time, is equal to t_O (Ω/Ω_O) where, $t_O = n/f_P$ and Ω_O, the solid beamwidth of the antenna (steradians), is approximately related to the antenna gain G by $G = 4\pi/\Omega_O$. Therefore, when n/f_P in Eq (1.6) is replaced with its equal, $4\pi t_S/\mathrm{G}\Omega$, The radar equation for a surveillance radar is obtained as

$$R_{max}^4 = \frac{P_{av} A_e \sigma E_i(n) F^4}{4\pi \, k T_o F_n (S/N)_1 L_s} \times \frac{t_s}{\Omega} \tag{1.7}$$

The radar designer has little control over the revisit time, t_S, or the angular coverage Ω, which are determined mainly by the job the radar has to perform. The radar cross section also is determined by the radar application. If a large range is required of a surveillance radar, the radar must have the necessary value of the product, $P_{av}A_e$. For this reason, a common

measure of the capability of surveillance radar is its power-aperture product. Note that the radar frequency does not appear explicitly in the surveillance radar equation. The choice of frequency, however, will enter implicitly in other ways.

Just as the radar equation for surveillance radar is different from the conventional radar equation of (1.6) or the simple radar equation of (1.3), each particular application of a radar generally has to employ a radar equation tailored to that specific application. When the radar echoes from land, sea, or weather clutter are greater than the receiver noise, the radar equation has to be modified to account for clutter being the limitation to detection rather than receiver noise. It can happen that the detection capability of radar might be limited by clutter in some regions of its coverage and be limited by receiver noise in other regions. This can result in two different sets of radar characteristics, one optimized for noise and the other optimized for clutter, and compromises usually have to be made in radar design. A different type of radar equation is also required when the radar capability is limited by hostile noise jamming [7].

1. 6 Radar Systems Classification

Depending on the desired information, radar sets have different qualities and technologies. One reason for these different qualities and techniques, radar sets are classified in Figure 1. 2 [8].

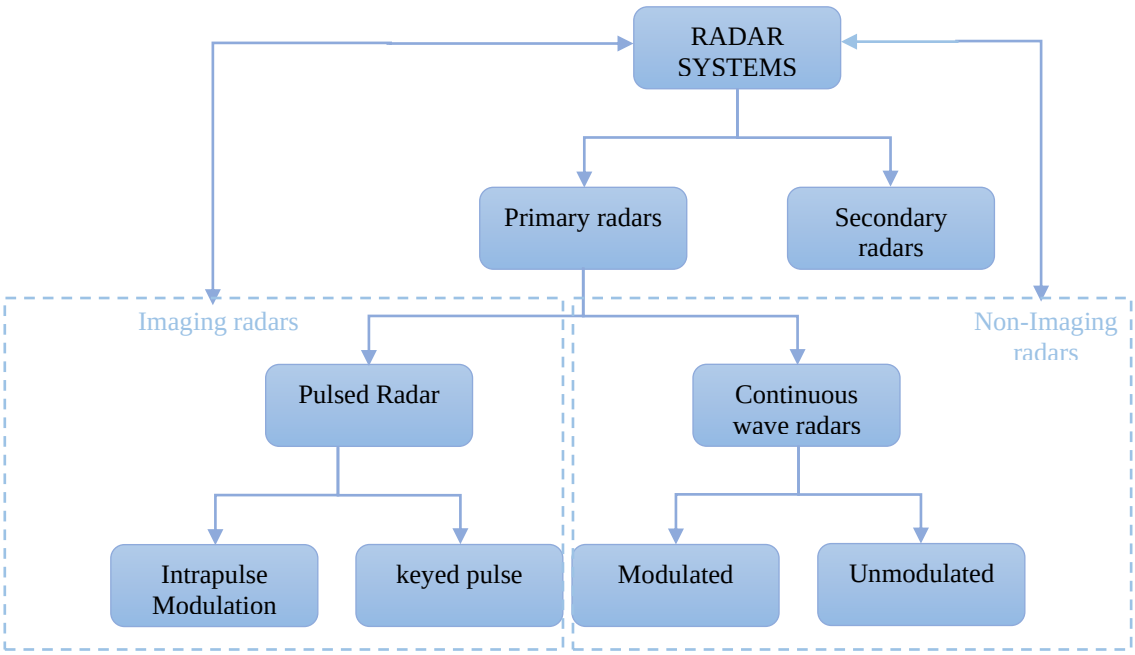

Figure 1.2 : Radar system classification

1. 6. 1 Imaging Radars / Non-Imaging Radars

Radar sets can be roughly divided into two categories: Imaging radar techniques (imaging radar) and non-imaging radar techniques (non-imaging radar). Imaging radar methods attempt to calculate a map-like image from the received information. Classic applications are weather radar and military air surveillance radar.

Non-imaging radar methods make their measurement results available as pure numerical values. Applications include some radar altimeters and speedometers. Non-Imaging Secondary Radar applications are immobilizer systems in some recent private cars [8].

1. 6. 2 Primary Radars

Primary radar (Primary Surveillance Radar or PSR) emits high-frequency pulses using an antenna, which are partially reflected by the flying object and return to the antenna. A receiver measures the time between the emission and return of the pulses. This duration and the direction of the pulse allow calculating the position of the flying object. There are primary radars that can determine positions in two dimensions (2D) (distance and azimuth) or three dimensions (3D) (distance, azimuth, altitude) [9].

1. 6. 3 Pulsed Radars

Pulsed radars emit high-frequency signal pulses with high power, and then wait for the echo of the transmitted signal for a certain time before transmitting a new pulse. Pulsed radars are generally used to detect targets within a certain volume of space and determine the distance and bearing, and in some cases, the speed of each target [10].

1. 6. 4 Continuous Wave Radars

Continuous wave (CW) radar is characterized by the continuous emission of waves, which can be frequency-modulated or not. The echoes are received and processed continuously. To prevent the emitted energy from directly entering the receiver and contaminating the returning signal, this type of radar emits and receives:

- Either using two different antennas (bi-static radar).
- Or measures the frequency difference between the two signals using a single antenna. Continuous wave radars are divided into two types:

(i) Unmodulated Continuous Wave Radars:

The emitted signal is constant in amplitude and frequency. Specialized in measuring speeds, unmodulated CW radars do not allow distance measurement. They are used, for example, by the police for speed control on roads.

(ii) Modulated Continuous Wave Radars:

The disadvantage of CW radars is their inability to measure distances because they do not produce the pulses that serve as timing markers. This problem can be solved by varying the emitted frequency. When an echo is received, the frequency of the signal reflected by the target can be measured. By referring to the moment when the same frequency value was emitted, it becomes possible to measure the time between emission and reception of this frequency, and thus the distance between the radar and the target [11].

1. 6. 5 Secondary Radars

Secondary radar operates according to a different principle: the target it illuminates generates (actively) response signals. The secondary radar transmits high-frequency pulses (called interrogations) that are not intended to be reflected, as the target is equipped with a transponder that receives and processes these pulses. Then, the transponder formats and emits a response message that can be received and decoded by the secondary radar. In the case of secondary radars, the necessary cooperation of the target (use of a transponder) allows for a significant reduction in the emitted power compared to primary radar offering an identical detection range [11].

1. 7 Applications of Radar System

Radars are used in countless applications, and their use in many of these applications has improved their performance. In fact, radar failure can completely paralyze their operation, as in aviation and maritime navigation systems. Radar is used in a wide range of applications, including land, air, ocean, and space. On land, it is primarily used to detect, locate, and track aircraft and space objects. At sea, it is used to locate ships and coastlines, while monitoring aircraft. On aircraft, radar serves as an essential tool for navigation and safety, as it can detect other aircraft, ships, and land vehicles, as well as mapping terrain and avoiding storms. In space, radar plays a critical role in spacecraft guidance and remote sensing of land and sea. The military has been the primary user of radar, contributing to its development costs, with

increasingly important civilian applications in maritime and aviation navigation (see Table 1.1).

Table. 1. 1 Application areas of radar systems

Category	Applications
Military Application	- Air defense (surveillance, missile guidance, weapon control) - Reconnaissance and targeting over land/sea - Ballistic missile and satellite detection - Battlefield surveillance and weapon control
Remote Sensing	- Weather observation (Nexrad, TDWR systems) - Spaceborne altimeter radar for geoid measurement - Ice navigation for ships - Soil moisture and crop status assessment
Air Traffic Control	- Airport Surveillance Radar (ASR) for air traffic monitoring - Airport Surface Detection Equipment (ASDE) for ground traffic control - Long-range Air Route Surveillance Radars (ARSR) for en-route traffic control
Other Applications	- Space exploration (**e.g:** Lunar surface imaging) - Marine radar for ship navigation - Police radar for speed detection - Ground-penetrating radar for archaeology and buried object detection - Ornithology and entomology studies

1. 8 Radar Clutter

Radars operate via transmission through a directional antenna. Objects within the field of view scatter radio frequency (RF) energy in all directions, some towards the receiving antenna. Reflections from the clutter are undesired, and may obscure signals from targets. In other words, radar clutter refers to a radar return from a target or targets that are unimportant to the radar emission. The identification and tracking of targets like planes, ships, or ground

vehicles is the purpose of many radar systems. These systems view clutter as a natural object that interferes with signals. There are two types of clutter; volume clutter and surface clutter. Figure 1. 3 presents the envelop detector of the clutter echoes having an intermediate frequency. The received echo, i.e., $q_r(t) = \tilde{A}\, cos(\omega_c t + \tilde{\varphi})$ has a random amplitude, $\tilde{A}$ and $\tilde{\varphi}$ a random phase. The magnitude or the envelop, X is obtained after calculating the in-phase I and quadrature Q components. Note that, the transmitted signal is, $q_e(t) = A\, cos(\omega_c t)$ with known A and carrier frequency, ω_c [12].

1. 8. 1 Volume Clutter

Volume clutter normally has a large extent and includes chaff, rain, snow, hail, birds, insects and other flying particles. Weather or rain clutter is easier to suppress than chaff, since rain droplets can be viewed as perfect small spheres. A resolution volume is shown in Figure 1. 4 and is approximated by [13]

$$V_W \approx \frac{\pi}{8}\theta_a \theta_e R^2 c\tau \tag{1.8}$$

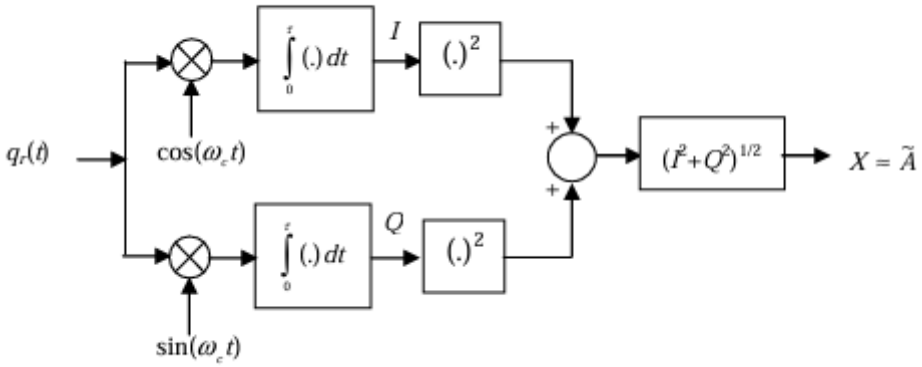

Figure 1. 3 Envelop detector of radar echoes with an intermediate frequency.

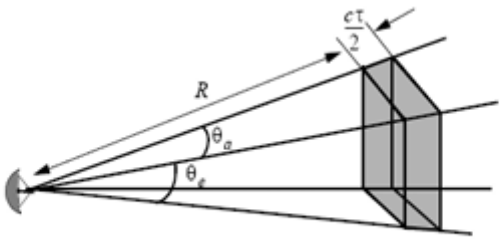

Figure 1. 4 Definition of a volume resolution.

Where θ_e and θ_a are, respectively, the antenna's beam width in azimuth and elevation, R is the range, c is the light speed and τis the sampling period which is the transmitted pulse width. The SCR for weather clutter is computed as

$$SCR = \frac{8\sigma_t}{\pi\theta_a\theta_e c\tau R^2 \sum_{i=1}^{N}\sigma_i} \tag{1.9}$$

Where σ_i is the i[th] rain droplet radar cross section (RCS) approximation. This type of clutter is modeled by Rayleigh (envelop detector is used) or exponential (square law detector is used) distribution where either I or Q component follows the normal distribution.

$$p(I) = p(Q) = \frac{1}{\sqrt{2\pi}\sigma} exp\left(-\frac{I^2}{2\sigma^2}\right) \tag{1.10}$$

In (1.10), σ^2 and $2\sigma^2$ denote respectively the variance and power of clutter. The output of the envelop detector, $X = \sqrt{I^2 + Q^2}$ is a random variable with Rayleigh distribution.

$$p(x) = \frac{x}{\sigma^2} exp\left(-\frac{x^2}{2\sigma^2}\right) \tag{1.11}$$

1. 8. 2 Surface Clutter

Surface clutter includes both ground (land) and sea-clutter, and is often called area clutter. Surface clutter includes trees, vegetation, ground terrain, man-made structures, and sea surface. Area clutter manifests itself in airborne radars in look-down mode. It is also a major concern for ground-based radars when searching for targets at low grazing angles. The grazing angle, ψ_g is the angle from the surface of the earth to the main axis of the illuminating beam, as illustrated in Figure 1. 5. The eliminated sea surface usually called the footprint is divided into many sub-range bins each of size (cτ/2) sec ψ_g . Consequently, the resolution area A_c is expressed as [13]

$$A_c = \mathrm{R}\theta_{3dB}\frac{\mathrm{c}\tau}{2}\sec\psi_g \tag{1.12}$$

Where $\sec(x) = 1/\cos(x)$.

This type of clutter may be subject to more distributions and statistics.

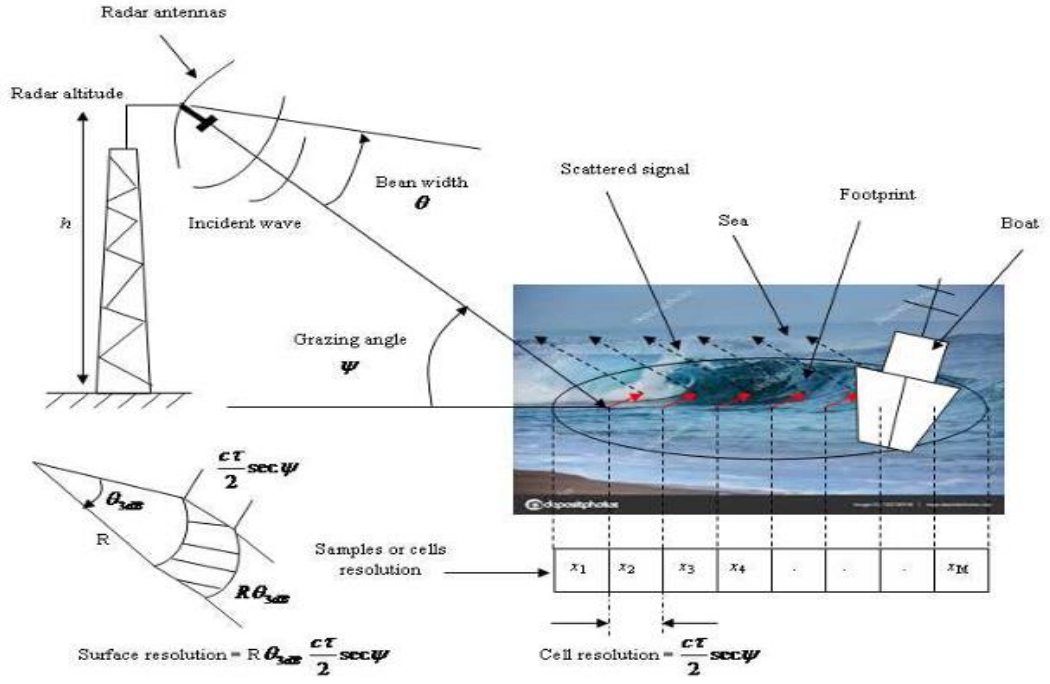

Figure 1. 5 Radar echoes from the sea surface (i.e., radar footprint) [13].

1. 9 Radar Targets

Most objects of interest, such as aircraft, ships, and many other types of irregular shapes, consist of groups of scattering facets that interfere with each other, and only statistical estimations are valid. These vary from spherical objects, which give a constant reflection to an irregular cluster of equally sized reflectors. The reflections from such clusters are constant during the short radar pulse length. If the radar frequency changes, there are different interference effects that depend on the probability distribution of the returns. This is the same distribution as if the object were rotated when measured at a constant frequency. Steady echoes are the easiest to detect and measure. Fluctuating echoes must be observed during a number of fading cycles to obtain a reasonable mean value for detection and measurement. Swerling proposed four statistical models of targets [13].

(i) Swerling case 1: In this case, the target echo power per pulse on any one scan is assumed to be constant, but these echo pulses are uncorrelated from scan to scan. An echo is then a scan-to scan fluctuation. The intensity, s of the entire pulse-train is independent and identically distributed (iid) with an exponential law [13].

$$p(\mathrm{s}) = \frac{1}{2\sigma_s^2} exp\left(-\frac{s}{2\sigma_s^2}\right) \tag{1.14}$$

where $2\sigma_s^2$ is the average RCS or SNR over all target fluctuations.

(ii) Swerling case 2: In this case, the fluctuations are faster than in case 1, and are assumed to be independent from pulse-to-pulse instead of from scan-to-scan. This is pulse-to-pulse fluctuation where the voltages of the echoes from the scatterer are parts of a pdf given in (1.14).

(iii) Swerling case 3: In this case, the fluctuations are scan-to-scan as in case 1, but the PDF is given by

$$p(s) = \frac{4s}{(2\sigma_s^2)^2} exp\left(-\frac{2s}{2\sigma_s^2}\right) \tag{1.15}$$

(iv) Swerling case 4: In this case, the fluctuations are pulse-to-pulse as in case 2, but the pdf is given by (1.15).

Note that in cases 1 and 2, the targets are assumed to be composed of a large number of independent scatterers (e.g., large aircraft). Cases 3 and 4 represent targets that have a single dominant non-fluctuating scatterer, together with other smaller independent scatterers (e.g., missiles). Observe that cases 1 and 2 targets produce signals whose envelopes are Rayleigh distributed, while cases 3 and 4 targets produce signals whose envelopes are chi-squared distributed [13].

Swerling cases 1 to 4 are the models most commonly used, even though other models have been developed. They are summarized in the chi-square, χ^2 target models family [13].

$$p(s) = \frac{1}{\Gamma(k)} \frac{k}{2\sigma_s^2} \left(\frac{ks}{2\sigma^2}\right)^{k-1} exp\left(-\frac{ks}{2\sigma_s^2}\right) \tag{1.16}$$

1. 10 False Alarm and Detection Probabilities

For any threshold setting there will be a corresponding probability that noise alone (and/or clutter) may exceed this threshold. When this happens, the radar will erroneously report a detected target at the corresponding position. The associated probability is therefore called the false alarm probability, P_{FA}. In a similar way, the probability of making a correct detection P_D can be associated for each chosen threshold. Since they both depend on the same threshold setting, it is clear that they are somehow related to each other. Assuming that at decision making instants the probability density functions of noise and noise + target

associated with the amplitude (y) distributions are $P_n(y)$ and $P_{n+s}(y)$, respectively, these probabilities are defined as

$$P_{FA} = \int_Y^\infty P_n(y)dy \tag{1.17}$$

$$P_D = \int_Y^\infty P_{s+n}(y)dy \tag{1.18}$$

Above relations indicate that,

• increasing the detection threshold Y will decrease both P_{FA} and P_D,

• decreasing the detection threshold Y will increase both P_{FA} and P_D,

which show that there is always a trade-off between improving detections and reducing false alarms. Since both P_{FA} and P_D change with detection threshold level it is possible to calculate a value of SNR which is required to achieve a certain detection probability P_D, for a given value of P_{FA} . In practice, P_{FA} is chosen first and then P_D is calculated/determined by using receiver operating characteristics (ROC) of the radar receiver. A typical ROC is illustrated in Figure 1. 6, where detection probability vs. SNR are plotted for different false alarm rates. Very low false alarm probabilities are used in radar systems as shown in the figure; as low as $P_{FA} = 10^{-6}$ to $P_{FA} = 10^{-8}$. If the noise amplitude distribution is assumed to be Gaussian ROC of radar can be obtained analytically. If not, (or if clutter determines CFAR detection threshold) then these graphs must be prepared either experimentally or numerically.

Calculation of the ROC of radar depends on a number of factors; including the statistical behavior of the target fluctuations and of the noise + clutter, the number of integrated pulses coherently and incoherently. All these are extensively studied and well documented in the literature [13].

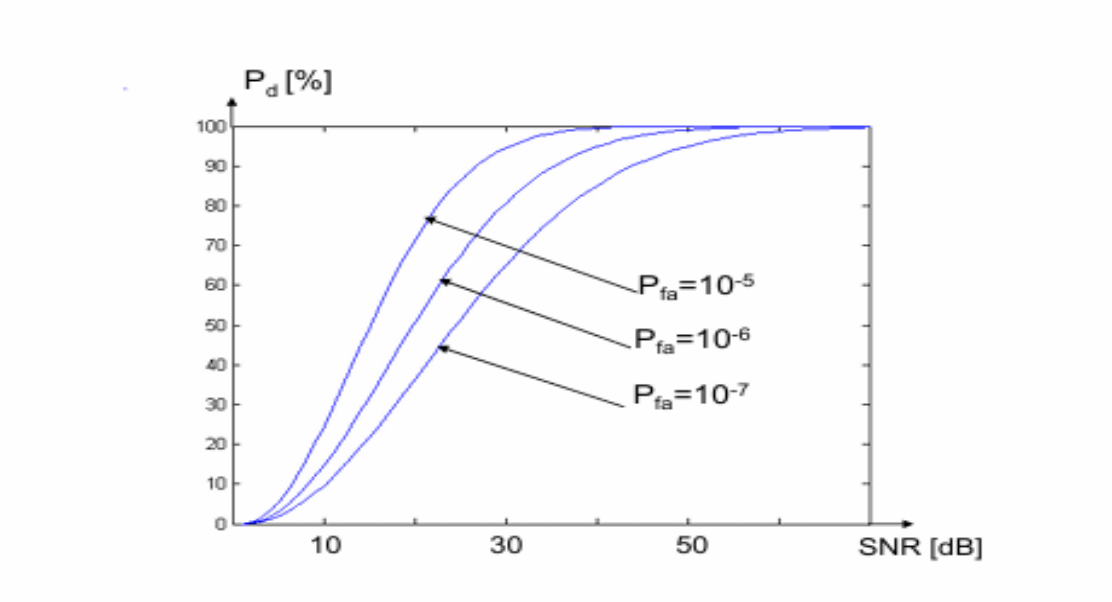

Figure 1.6 Typical radar ROC graph.

1. 11 Conclusion

The present Chapter reviewed firstly the history of radar systems and their evolution over time, beginning with military uses and then transitioning to civilian applications such as weather monitoring, air traffic control, and maritime surveillance. The basic components of radar systems, such as the transmitter, receiver, and antenna, are explained, and how they operate by transmitting radio waves and receiving reflections to determine distance, speed, and direction were presented. Radar equations, classification concepts, and various applications were also discussed. Clutter and targets types were given by their probability density functions, including volume clutter, area clutter and Swerling targets. Chapter 2 will continue this trend by improving radar models to deal with sea clutter.

Chapter 2

Modeling of High-Resolution Sea-Clutter

Abstract:

In this Chapter, we aim to obtain accurate fitting to IPIX sea clutter using single look mixture generalized gamma distributions. To assess modeling results, comparison purposes are curried out against standard distributions such as GG, K, K+noise CG-LNT, CG-LNT+noise, and mixture GG. Parameters finding of underling models are obtained by means of LSA approach. Experimental studies show that the Trimodal GG model can fit accurately most scenarios of IPIX database.

Chapter outline:

2. 1 Introduction……..……..……23

2. 2 Sea-Clutter Distributions…….…….…….…..…..23

2. 3 Mixture GG Clutter Model ……..…….……..….….26

2. 4 Parameter Estimation…….……..….…….27

2. 5 Experimental Results……..….….….29

2. 6 Conclusion…….……..…..37

2. 1 Introduction

Statistical modeling of radar clutter amplitudes or intensities is of great importance for many signal processing techniques in particular the construction of CFAR detection schemes [14]. In maritime surveillance radars, sea clutter of quite low resolution is modeled previously by the Rayleigh distribution in the amplitude domain. However, this model is restricted by sea surface conditions and radar system parameters. These limitations are then encountered by the use of compound Gaussian class distributions where gamma, inverse gamma, log-normal, and inverse Gaussian variates are taken into account for the texture component (ie., average of clutter power) [15]. For more improvement of the modeling performances, Trimodal family of continuous probability distributions on the positive real line has been recently validated by means of Ingara and IPIX databases [16, 17].

In order to obtain an accurate fit with sea reverberation data, we propose, in this Chapter, a Trimodal GG disturbance model. The NLSA approach is used to avoid computational issues associated with the maximum likelihood estimator (MLE) and moments-based estimators. Tests based on Recorded real life IPIX database are worked out to assess the proposed and standard CG-LNT, GG, CG-LNT+noise, K+noise and mixture GG distributions. It is show that the Trimodal GG distribution is validated to be in qualitative agreement with different cell resolutions of available IPIX database.

The Chapter is organized as follows. Section 2. 2 presents the GG distribution and recalls some standards statistical distributions that will used for comparison purposes. Then, the mixture GG with two and three GG distributions are given with the LSA estimation method of their parameters in Section 2. 3. Section 2. 4 assesses the best fitting to IPIX real data using proposed and conventional distributions. Finally, Section 2. 5 highlights main remarks about the obtained modeling results.

2. 2 Sea-Clutter Distributions

In sea environment, radar returns has complicate characteristics such as non-uniform, non-Gaussian, non-stationary, etc. For this reason, the modeling of surface clutter in high-resolution radar systems is the first research issues in CFAR detection schemes [2]. Targets such as ships, boats, aircrafts, etc that are moved over sea surface are detected with a CFAR behavior. The purpose of this Section evokes the modeling of sea clutter using GG, *K*, *K*+noise, CG-LNT and CG-LNT+noise distributions.

2. 2. 1 Generalized Gamma Clutter Model

From the open literature, a three-parameter family class of distributions is useful for sea reverberation data [18]. For instance, a single look three parameter generalized gamma (GG) probability density function (PDF) of the amplitude, *X*, is given by [18]

$$p_X(x;a,b,\nu) = \frac{b}{a\Gamma(\nu)}\left(\frac{x}{a}\right)^{b\nu-1} exp\left(-\left(\frac{x}{a}\right)^{b}\right) \tag{2.1}$$

Where $\Gamma(.)$ is the gamma function, a is a scale parameter, b and $\boldsymbol{\nu}$are two shape parameters. Values of b and ν between '0' and 'infinity' assimilate the spikiness degrees of the clutter. The complementary cumulative distribution function (CCDF) is obtained from (2.1) as

$$\begin{aligned} CCDF(T;a,b,\nu) &= \int_{T}^{+\infty} p_X(x)dx \\ &= 1 - \frac{b}{a\Gamma(\nu)}\int_0^T \left(\frac{x}{a}\right)^{b\nu-1} exp\left(-\left(\frac{x}{a}\right)^{b}\right)dx \end{aligned} \tag{2.2}$$

Where T is a threshold. If we set, $t = (x/a)^b$ and $\frac{dt}{dx} = \frac{b}{a}(x/a)^{b-1}$, (2.2) becomes

$$\begin{aligned} CCDF(T;a,b,\nu) &= 1 - \frac{1}{\Gamma(\nu)}\int_0^{(T/a)^b} t^{\nu-1}e^{-t}dt \\ &= 1 - \gamma((T/a)^b,\nu) \end{aligned} \tag{2.3}$$

Where $\gamma(.,.)$is the lower incomplete gamma function. Under the assumption of independent and identically distributed (iid) samples of the clutter range profile (CRP), the expression of moments of order, r is given by

$$\begin{aligned} \langle \boldsymbol{x^r} \rangle &= \int_{\boldsymbol{0}}^{+\infty} \boldsymbol{x^r p_X(x)dx} \\ &= \boldsymbol{a^r \frac{\Gamma(\nu + r/b)}{\Gamma(\nu)}} \end{aligned} \tag{2.4}$$

where$\langle . \rangle$ denotes expectation and the moment counterpart is, $\langle x^r \rangle \approx \hat{\mu}_r = \frac{1}{M}\sum_{i=1}^{M} x_i^r$.

2. 2. 2 *K*-Clutter Model Plus Noise

On the other hand, the *K*-distribution is a class of a two-parameter CG models which is obtained from the combination of Rayleigh and texture components distributions given by, $p_X(x/y)$ and $p_Y(y)$ respectively [19]

$$\begin{cases} p_X(x|y) = \frac{2x}{y} exp\left(-\frac{x^2}{y}\right) \\ p_Y(y) = \frac{b^{\nu} y^{\nu-1}}{\Gamma(\nu)} exp(-by) \end{cases} \tag{2.5}$$

Where, b is the scale parameter and, $\boldsymbol{\nu}$, is the shape parameter. Using (2.5), the overall *K*-distribution is calculated by

$$p_X(x) = \int_0^{+\infty} p_X(x|y)p_Y(y)dy$$

$$= \frac{2b^\nu}{\Gamma(\nu)} \left(\frac{x^2}{b}\right)^{\frac{\nu-1}{2}} K_{\nu-1}(2\sqrt{b}x) \quad (2.6)$$

Where $K_{\nu-1}(.)$ is the modified 'Bessel' function of the second kind of order ν-1. The corresponding CCDF is

$$CCDF(T; b, \nu) = \frac{2b^\nu}{\Gamma(\nu)} \left(\frac{T^2}{b}\right)^{\frac{\nu}{2}} K_\nu\left(2\sqrt{b}T\right) \quad (2.7)$$

and the moments of order, r is

$$\langle x^r \rangle = \frac{b^{-r/2}\,\Gamma(1+r/2)\Gamma(\nu+r/2)}{\Gamma(\nu)} \quad (2.8)$$

If the thermal noise is not neglected in the reception chain with a noise power, p_n, the speckle component distribution will be

$$p_X(x|y) = \frac{2x}{y+p_n} exp\left(-\frac{x^2}{y+p_n}\right) \quad (2.9)$$

The global PDF of K-clutter plus noise is given n integral form

$$p_X(x) = 2\frac{b^\nu x}{\Gamma(\nu)} \int_0^{+\infty} \frac{y^{\nu-1}}{y+p_n} exp\left(-by - \frac{x^2}{y+p_n}\right) d\,y \quad (2.10)$$

where the corresponding CCDF is

$$CCDF(T; b, \nu, p_n) = \frac{2b^\nu}{\Gamma(\nu)} \int_0^{+\infty} y^{\nu-1}\, exp\left(-by - \frac{T^2}{y+p_n}\right) d\,y \quad (2.11)$$

In this case, the expression of moments of order, r is

$$\langle x^r \rangle = \frac{2\Gamma(1+r/2)b^\nu}{\Gamma(\nu)} \int_0^{+\infty} (y+p_n)^{r/2} y^{\nu-1}\, exp(-by)\, dy \quad (2.12)$$

2. 2. 3 CG-LNT Clutter Model

This model is also a class of a two-parameter Compound Gaussian distribution obtained from Rayleigh and log-normal models of the speckle and the texture components respectively [20]

$$p_X(x) = \frac{2x}{\sqrt{2\pi\sigma^2}} \int_0^{+\infty} y^{-2}\, exp\left(-\frac{[\ln(y/\delta)]^2}{2\sigma^2} - \frac{x^2}{y}\right) d\,y \quad (2.13)$$

Where, $\ln(\delta)$ and σ represent respectively the mean and the standard deviation of the random variable, X. The equivalent CCDF is

$$CCDF(T; \delta, \sigma) = \frac{1}{\sqrt{2\pi}\sigma} \int_0^{+\infty} y^{-1}\, exp\left(-\frac{[\ln(y/\delta)]^2}{2\sigma^2} - \frac{T^2}{y}\right) d\,y \quad (2.14)$$

The moment of order, r is

$$\langle x^r \rangle = \delta^{r/2}\Gamma(1+r/2)\exp\left(\frac{1}{2}\left(\frac{r\sigma}{2}\right)^2\right) \tag{2.15}$$

If the noise power is added to the clutter power, y, (2.13) becomes

$$p_X(x) = \frac{2x}{\sqrt{2\pi}\sigma}\int_0^{+\infty}\frac{y^{-1}}{y+p_n}exp\left(-\frac{[\ln(y/\delta)]^2}{2\sigma^2}-\frac{x^2}{y+p_n}\right)d\,y \tag{2.16}$$

The CCDF in this case will be

$$CCDF(T;\delta,\sigma) = \frac{1}{\sqrt{2\pi}\sigma}\int_0^{+\infty} y^{-1}\,exp\left(-\frac{[\ln(y/\delta)]^2}{2\sigma^2}-\frac{T^2}{y+p_n}\right)d\,y \tag{2.17}$$

The moment of order, r is also given in integral form

$$\langle x^r \rangle = \frac{2\Gamma(1+r/2)}{\sqrt{2\pi}\sigma}\int_0^{+\infty}(y+p_n)^{r/2}y^{-1}\,exp\left(-\frac{[\ln(y/\delta)]^2}{2\sigma^2}\right)dy \tag{2.18}$$

2. 3 Mixture GG Clutter Model

In some cases, distributions given in Section 2.2 do not fit real data that follow two or more densities [16, 17]. This is happen when radar echoes are observed from small range cells where the CCDF curves have a certain number of inflexion points. For this reason, a general mixture generalized gamma (GG) distribution could be able to describe this kind of data scenarios given by

$$p_X(x;k_i,a_i,b_i,\nu_i) = \sum_{i=1}^{n} k_i\frac{b_i}{a_i\Gamma(\nu_i)}\left(\frac{x}{a_i}\right)^{b_i\nu_i-1}exp\left(-\left(\frac{x}{a_i}\right)^{b_i}\right) \tag{2.19}$$

where k_i, i = 1, …, n is probability (i.e., $\sum_{i=1}^{n} k_i = 1$) and n the number of GG distributions. If n = 3, (2.19) is labeled Trimodal GG distribution and its corresponding CCDF is written as

$$CCDF(T;k_i,a_i,b_i,\nu_i) = \sum_{i=1}^{n} k_i\left(1-\gamma((T/a_i)^{b_i},\nu_i)\right) \tag{2.20}$$

Moments formula of order, r is

$$\langle x^r \rangle = \sum_{i=1}^{n} k_i\,a_i^r\frac{\Gamma(\nu_i+r/b_i)}{\Gamma(\nu_i)} \tag{2.21}$$

The above equations (2.19), (2.20) and (2.21)) have 4n-1 parameters, n discrete scale parameters,a_i, n discrete shape parameters b_i, n discrete shape parameters ν_i and n-1 probabilities k_i. Note that, (2.19), (2.20) and (2.21)) represent general cases of trimodal distributions given in [16, 17] for a single look case transmission. If we set, $a_i = a$ for i = 1, …, n, the number of parameters is reduced to 3n.

2. 4 Parameter Estimation

The maximum likelihood estimator (MLE) procedure for K+noise, CG-LNT+noise and mixture GG distributed parameters is executed numerically and expends more time for convergence. To overcome this complexity, we refer in this work to the use of the NLSA approach [21]. Note that, the GG distributed parameters can be estimated by means of the following fractional order moments given by

$$\begin{cases}\langle x^{r+1}\rangle = a^{r+1}\frac{\Gamma(\nu+(r+1)/b)}{\Gamma(\nu)} \\ \langle x\rangle\langle x^{r}\rangle = a^{r+1}\frac{\Gamma(\nu+1/b)\Gamma(\nu+r/b)}{\Gamma(\nu)^2}\end{cases} \tag{2.22}$$

Combination of the two equations in (2.22) gives

$$\frac{\langle x^{r+1}\rangle}{\langle x\rangle\langle x^{r}\rangle} = \frac{\Gamma(\nu)\Gamma(\nu+(r+1)/b)}{\Gamma(\nu+1/b)\Gamma(\nu+r/b)} \tag{2.23}$$

Note that, the parameter search in (2.23) is reduced to two dimensions instead of three in (2.22).

For the case of mixture GG distribution, the fitness function is given as the sum of quadratic errors between empirical and theoretical CCDF quantities

$$Fitness_{CCDF} = \sum_{j=1}^{m_1}\left[real_{CCDFj} - \sum_{i=1}^{n} k_i\left(1-\gamma((T/a_i)^{b_i},\nu_i)\right)\right]^2 \tag{2.24}$$

Subject to $a_i > 0$, $b_i > 0$, $\nu_i > 0$ and $\sum_{i=1}^{n} k_i = 1$. m_1 and m_2 denote numbers of selected points in the curves of the objective function. To minimize again the search space dimension to 3*n*-1, we utilize the clutter mean in the estimation procedure so that

$$\begin{cases}a_i = a \\ a = \langle x\rangle\left[\sum_{i=1}^{n} k_i\frac{\Gamma(\nu_i+1/b_i)}{\Gamma(\nu_i)}\right]^{-1}\end{cases} \tag{2.25}$$

Simplex minimization (SM) was widely used for solving a variety of optimization problems. The Nelder-Mead (NM) simplex algorithm [22], published in 1965, is an enormously popular search method for multidimensional unconstrained optimization. No derivative of the cost function is required, which makes the algorithm interesting for noisy problems. The NM algorithm falls in the more general class of direct search algorithms. It maintains a simplex which are approximations of an optimal point. The vertices are sorted according to the objective function values. The algorithm attempts to replace the worst vertex with a new point, which depends on the worst point and the centre of the best vertices. The goal of this part is to provide a NM direct search optimization method to solve the above constrained optimization problem given by (2.24).

This algorithms is based on the iterative update of a simplex made of m + 1 points$S = \{Vi\}$, i = 1, 2, …, m+1. Each point in the simplex is called a vertex and is associated with a function value, $f_i = f(V_i)$. It uses four parameters: the coefficient of refection,$\rho > 0$, expansion,$\chi > 1$ with,$\chi > \rho$, contraction $0 < \gamma < 1$ and shrinkage, $0 < \sigma < 1$. The standard values of these coefficients are, $\rho = 1$, $\chi = 2$, $\gamma = 0.5$and $\sigma = 0.5$. Moves of NM simplex are executed according to five main operators; Reflection, Expansion, Inside contraction, Outside contraction, Shrink after inside contraction and Shrink after outside contraction.

These components are interpreted by mathematical equations that are well detailed in [22]. Figure. 2. 1 summarizes the different steps of the optimization of (2.24) with constraint using the SM based on the N-M algorithm.

2. 5 Experimental Results

In this Section, we investigate the modeling of real IPIX using proposed and existing distributions given in Section 2. 3. From the data, respective parameters are estimated by the LSA method highlighted in Figure 2. 1 and comparisons are pointed up by the difference between theoretical and empirical CCDFs.

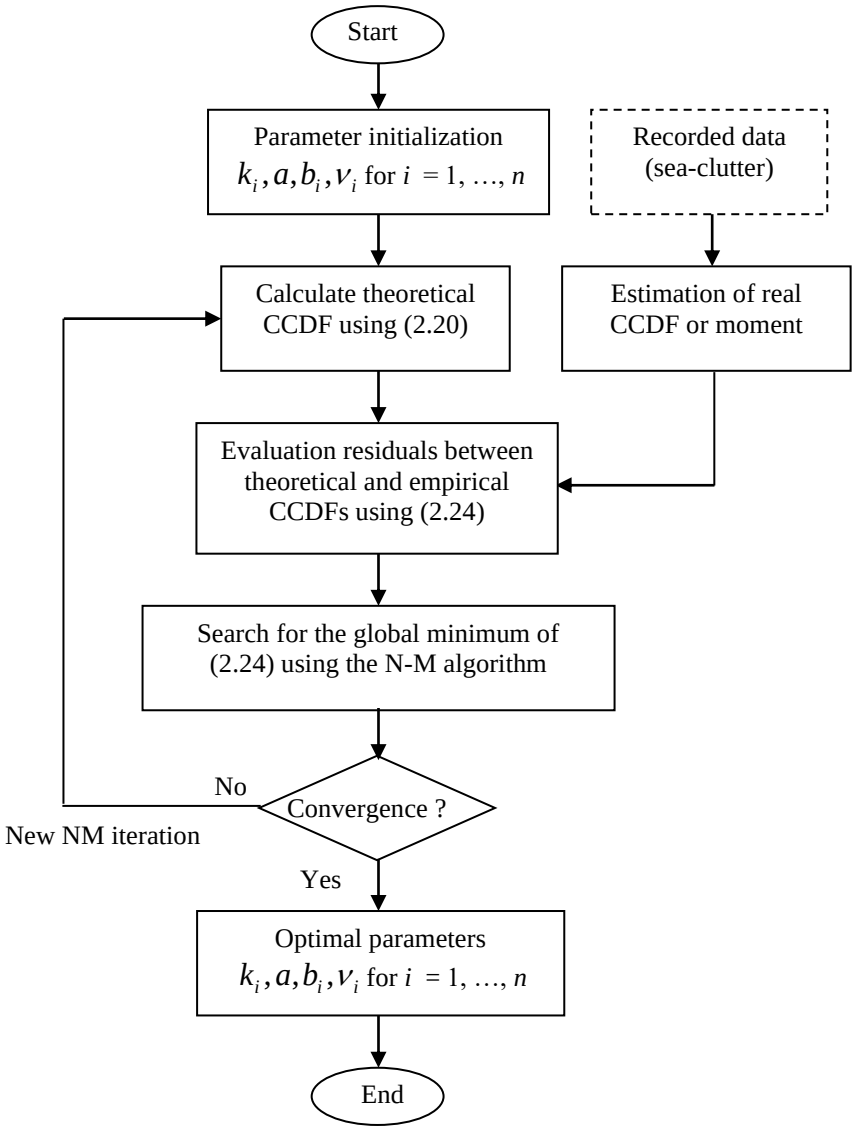

Figure. 2. 1 Flowchart of the simplex minimization algorithm of (2.24)

2. 5. 1 Characteristics of IPIX Database

The McMaster IPIX radar sea clutter database is available with different sea and radar parameters [23]. It is intended for researchers to assess their algorithms developed in radar research community. Among these include statistical models of sea surface, estimators of parameters of clutter distributions and targets CFAR schemes.

The IPIX radar system is fully coherent X-band radar with dual transmit/receive antennas polarization, frequency agility and stare/surveillance mode. The IPIX data used in this thesis concerns high resolution measurements collected in Grimsby during winter 1998, on the shore of Lake Ontario. Graphical display of all 222 datasets and pictures including radar return plots and time Doppler spectra are available in [23]. Specifically, there are co-polarizations, HH and VV (Lpol), and cross-polarizations, HV and VH (Xpol), coherent reception, leading to a quadruplet of I and Q values for co-pol and cross-pol. Through the recordings, the radar was transmitting with a PRF of 1000 Hz and a pulse length of 0.06 us. The received IPIX data is treated by the arrival order and registered in a (60000x34) matrix where 34 denotes the number of range cells and 60000 is the number of pulses.

In the following, we focus our analysis on the datasets 84, 85 and 86 which correspond to the range resolutions 30m, 15m and 3m respectively. Characteristic features of the above IPIX data sets are summarized in the following Table [23].

The IPIX radar files are stored in Unidata's NetCDF file format (not to be confused with the NSSDC's CDF file format). This format is ideal for efficient storage of multidimensional array data. The data are easily imported into Matlab using the freely available MexCDF toolbox. The following six steps are given to start working with the data in Matlab:

Step1: Open the Matlab and specify the current folder source which contains real data given as compressed cdf files.

Step2: Select all folders and files.

Step3: Click on the right button and choose ‘selected folders’ and then ‘selected folders and subfolders’

Step4: Choose for example the data file ‘19931118_023604_stareC0000.cdf’ and execute the Matlab command, nc=netcdf('19931118_023604_stareC0000.cdf').

Step5: Execute the Matlab command, ipixinfo(nc).

Step6: Download the m-file ipixload.m using the following Matlab command:
[I,Q,meanIQ,stdIQ,inbal] = ipixload(nc,pol,rangebin,mode).

For the specification of pol, rangebin and mod, these information are given after the execution of ipixinfo(nc). From the above example of the Dartmouth data cdf file we have:

Pol = A (ie., 'HV' or 'VH')
Rangebin = 14
Mode = 'auto'
The in-phase I and quadrature Q components of envelop, X are given by the following Matlab routine:

```
[I,Q,meanIQ,stdIQ,inbal] = ipixload(nc,'VH',1:14,'auto');
X = I+jQ;
```

The sea clutter intensity will be

```
z = abs(X(:,6)).^2;
```

For more information, please consult [22].

Table. 2. 1 Properties of IPIX recorded data collected at Grimsby, Ontario, Canada [24].

Dataset	**19980204_220849 (file 84) Resolution 30m**	**19980204_223220 (file 85) Resolution 15m**	**19980204_223506 (file 86) Resolution 3m**
Date and time	02/04/1998 22:08:49	02/04/1998 22:32:20	02/04/1998 22:35:06
Number of range cells	34	34	34
Start range	3201 m	3201 m	3201 m
Range resolution	30m	15m	3m
Number of sweeps	60000	60000	60000
Sample per cell	60000	60000	60000
PRF	1 KHz	1 KHz	1 KHz
RF-frequency	9.39 GHz	9.39 GHz	9.39 GHz
Radar and wave geometry	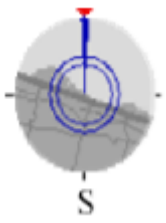		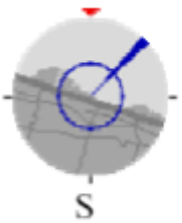

2. 5. 2 Modeling Assessments

In this Subsection, IPIX real-life datasets are used to obtain the following empirical and theoretical CCDFs.

Our first modeling study begins by plotting the different CCDFs curves as a function of the normalized threshold, *T* in dB for cases of high resolution of 3m, HH radar antennas polarization and 9th range cell as shown in Figure 2. 2. It pinpointed out that the best fit to real CCDF is approved by the use of the proposed Trimodal GG CCDF. Moreover, the mixture of 2 GG model approximates also this case of the data. It is noticed that *K*+noise, CGLNT+noise and GG have bad modeling performances, because the empirical CCDF has some inflexion points. Figures 2. 3 and 2. 4 depict the corresponding CCDFs when the 17th and 30th range cells are selected with HH polarization and a resolution of 3m. Also, mixture models including Trimodal GG and mixture of 2 GG distributions are well adapted for this type of the data containing some inflexion points. The modeling results are now depicted in Figure 2. 5 for cases of VV antennas polarization, resolution of 3m and 12th range cell. The Trimodal GG CCDF has always a goodness fit to real data compared to the rest of the distributions. As shown in Figures 2. 6 and 2. 7 for the case of HH and VV polarizations, 3rd and 15th range resolutions and resolutions of 3m and 15m respectively, all theoretical distributions have almost the same modeling results, since the inflexion points are not appeared in the empirical CCDF. On the other hand, Figure 2. 8 illustrates that the *K*+noise model demonstrates the best fit to real data with respect to other CCDFs curves obtained from HH polarization, 4th range cell and a resolution 30m. Finally, experimental modeling results presented in Figure 2. 9 reveal that GG, 2 GG and Trimodal GG have the best tail regression to real CCDF curve for cases of 22nd range cell, VV antenna polarization and a resolution of 30m.

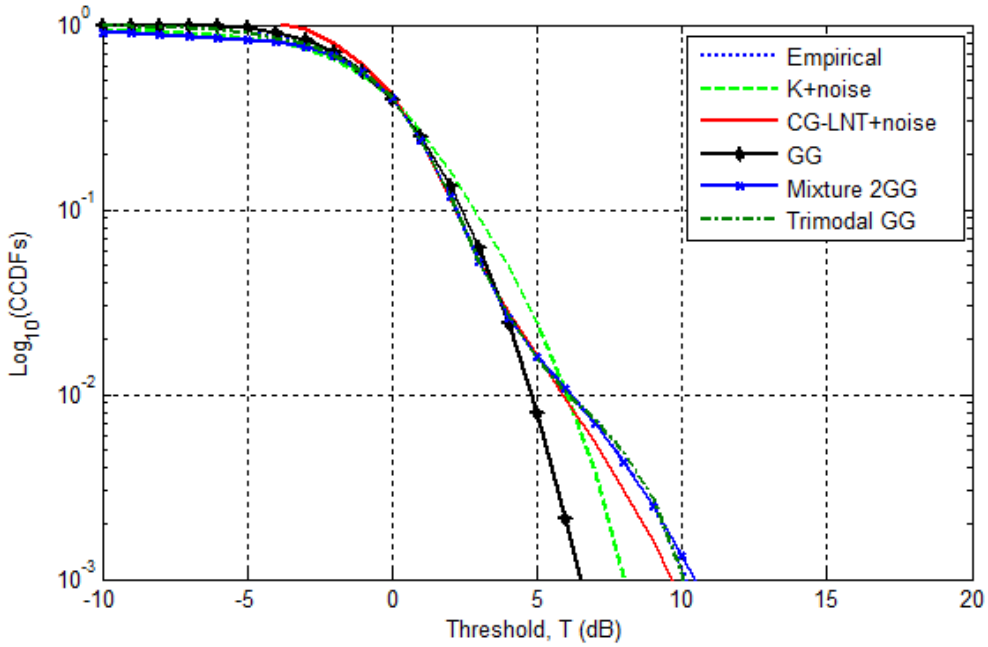

Figure 2. 2 Modeling of IPIX real data for HH polarization, 9th range cell and 3m resolution.

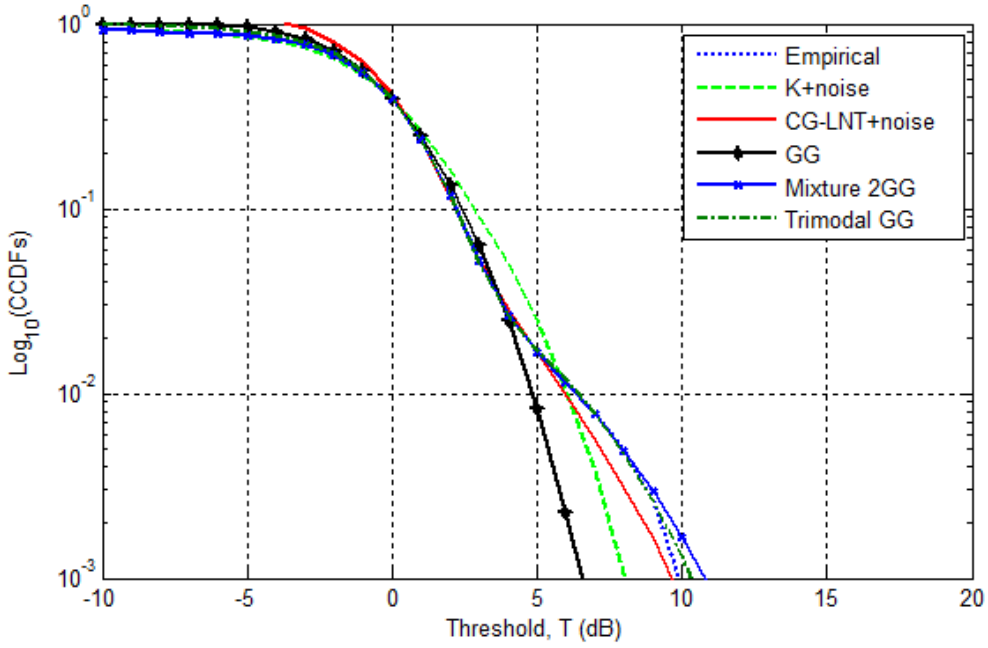

Figure 2. 3 Modeling of IPIX real data for HH polarization, 17th range cell and 3m resolution.

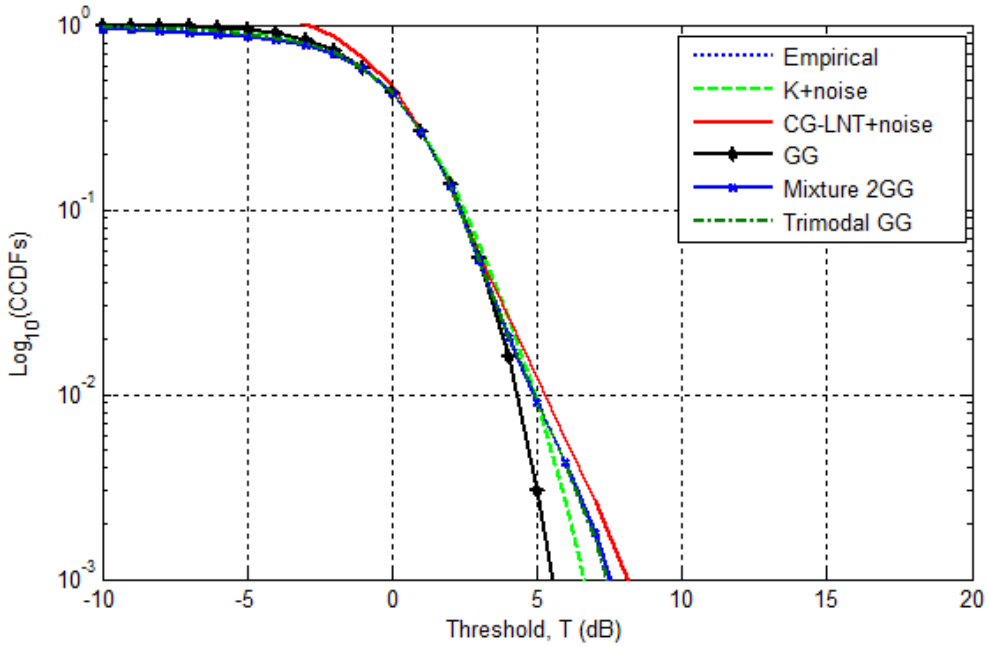

Figure 2. 4 Modeling of IPIX real data for HH polarization, 30th range cell and 3m resolution.

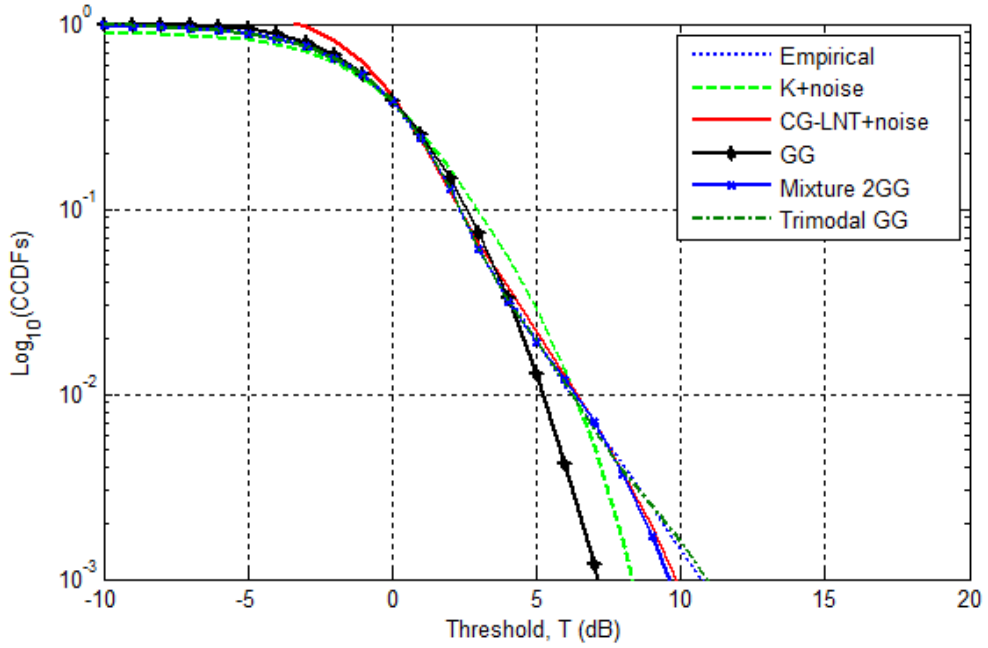

Figure 2. 5 Modeling of IPIX real data for VV polarization, 12th range cell and 3m resolution.

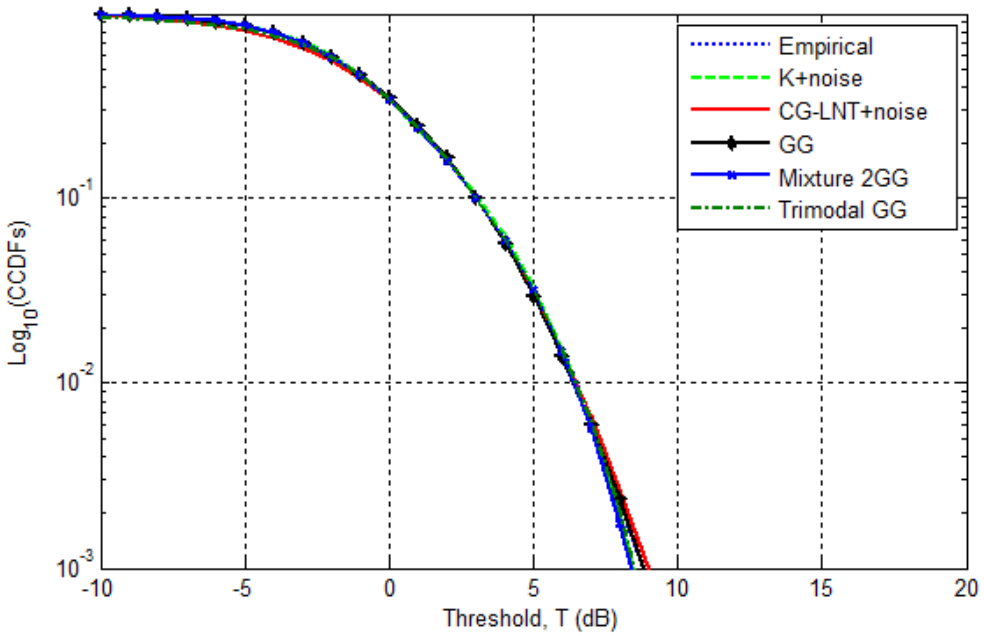

Figure 2. 6 Modeling of IPIX real data for HH polarization, 3rd range cell and 15m resolution.

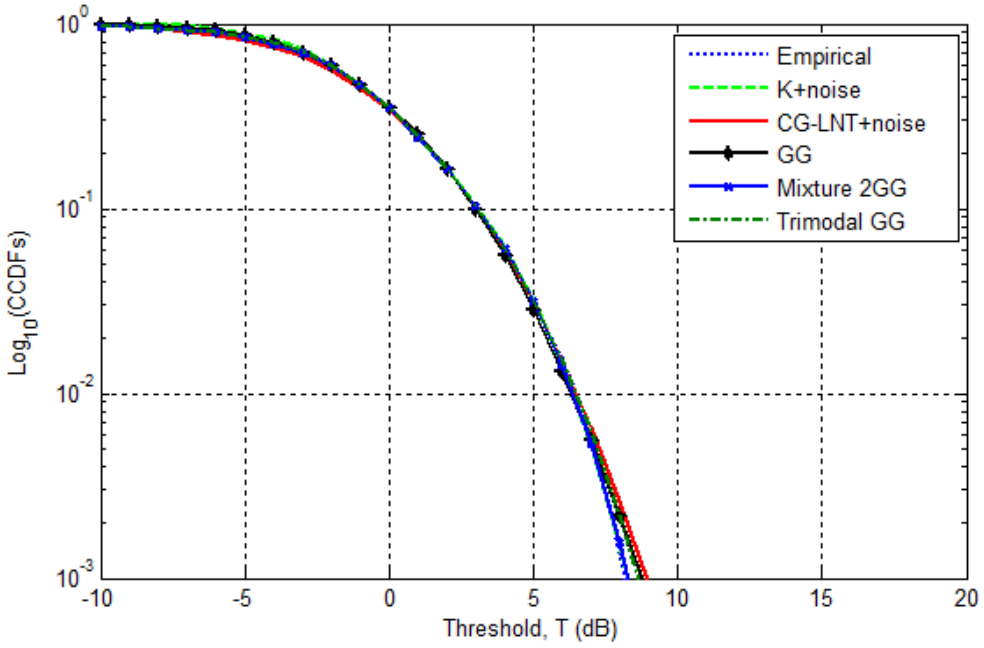

Figure 2. 7 Modeling of IPIX real data for VV polarization, 15th range cell and 15m resolution.

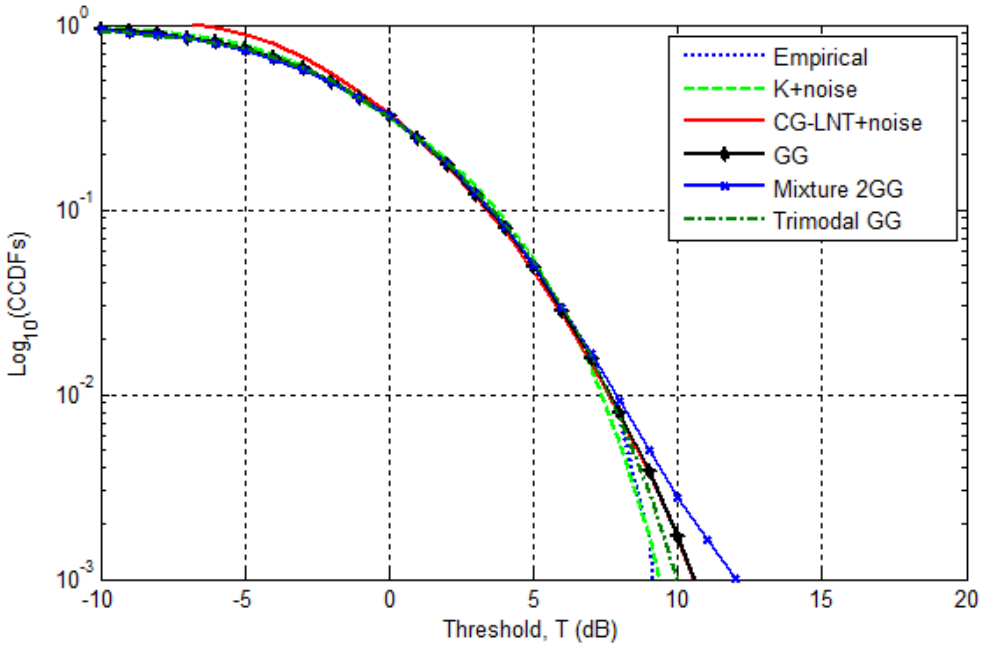

Figure 2. 8 Modeling of IPIX real data for HH polarization, 4th range cell and 30m resolution.

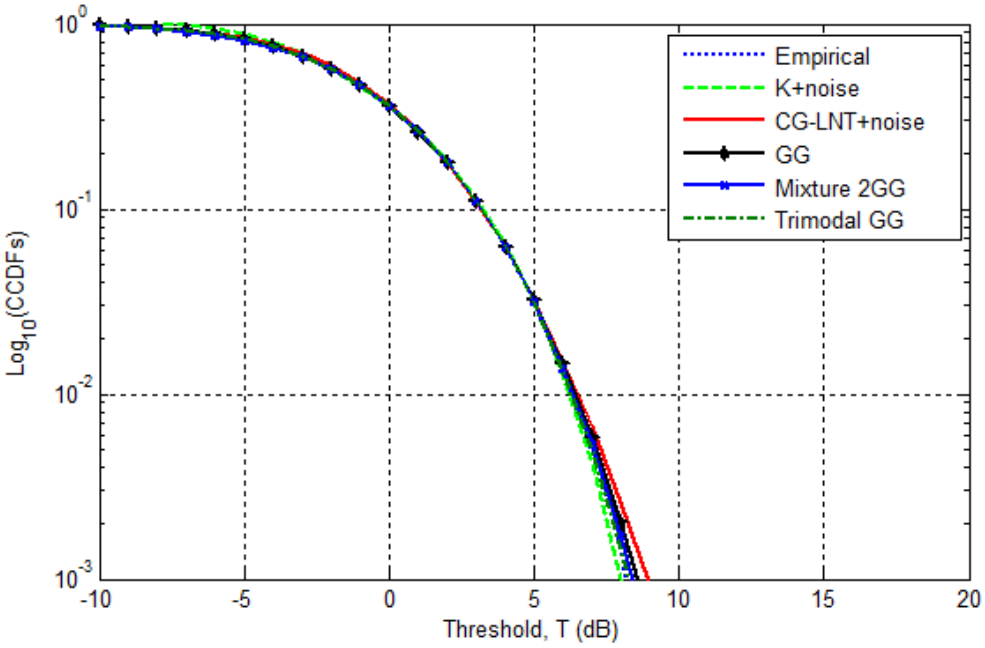

Figure 2. 9 Modeling of IPIX real data for VV polarization, 22th range cell and 30m resolution.

2. 6 Conclusion

Trimodal generalized gamma distribution were introduced in this Chapter as a correct description of sea reverberation data. The latter was given form a mixture of three GG distributions. For comparison purposes, classical distributions like *K*+noise, CG-LNT+noise and GG were considered after utilizing the LSA estimation method for parameters finding of underling models. Experiments study showed that the Trimodal GG distribution is suitable for modeling IPIX data in most cases. To demonstrate this, several scenarios of IPIX samples with different range resolutions and antennas polarizations were taken into account. The computational time associated with the proposed model is relatively high owing to the fact that they search eight dimensional spaces. To conclude, the application of the Trimodal GG distribution is a novel approach to modeling IPIX radar echoes. In fact, this model should produce excellent tail fitting of the other types of sea echoes.

Chapter 3

CFAR Detection in CG-LNT Clutter and Multiple Targets Situations

Abstract:

CFAR detection in homogeneous and heterogeneous CG-LNT distributed sea-clutter is studied in this Chapter. Detectors based on logt-, OS-, WH-, WHOS, WHWH- and WHWHOS-CFAR are given by means of their test statistics. Performance analysis of underling CFAR procedures is investigated using both simulated and real IPIX databases. The robustness of each CFAR detector is tested by changing values of the standard deviation clutter parameter and the number of outliers (interfering targets).

Chapter outline:

3. 1 Introduction……..…….…....……39

3. 2 WHWHOS-CFAR Detector…….…….……..39

3. 3 Detection Performance Comparisons…….…....……...41

3. 4 Conclusion……..……...…...56

3. 1 Introduction

This Chapter deals with the problem of targets CFAR detection embedded in homogeneous and heterogeneous CG-LNT distributed clutter. As discussed in Chapter 2, the latter is expressed in terms of two parameters; standard deviation parameter and scale parameter. It possesses a strong ability to model various sea clutter scenarios. The performances of logt-, OS-, WH-, WHOS-, WHWH- and WHWHOS-CFAR algorithms are examined in terms of standard deviation parameter. In the presence of interfering targets OS-, WH-, WHOS- WHWH- and WHWHOS-CFAR CFAR detectors are considered where the CFAR properties are also investigated as a function of clutter parameters.

The Chapter is organized as follows. Section 3. 2 highlights the operation of standard and proposed WHWHOS-CFAR detectors operating in homogeneous and heterogeneous background. Section 3. 3 concerns the comparison purposes of CFAR properties and detection probabilities of the different CFAR detectors presented in Section 3. 2. Finally, Section 3. 4 summarizes the main results obtained in this Chapter.

3. 2 WHWHOS-CFAR detector

The two parameters CG-LNT distribution is used to characterize sea-clutter statistics [20]. In this Section, we apply some CFAR procedures that can be operated in CG-LNT clutter without thermal noise. Recent tests statistics that are also useful in the presence of interfering targets embedded in several sea-clutter are obtained from a general test statistic [25]. The latter is given in terms of two non-negative scale invariant functions $g(.)$ and $h(.)$ selected as a function of clutter samples so that [25, 26].

$$X_0 \underset{H_0}{\overset{H_1}{>}} \underbrace{g(X_1, X_2, ..., X_N) e^{th\left(\log\left(\frac{x_1}{g(X_1, X_2, ..., X_N)}\right), ..., log\left(\frac{x_N}{g(X_1, X_2, ..., X_N)}\right)\right)}}_{T} \tag{3.1}$$

Where X_0 is the Cell Under Test (CUT), The target is declared present (i.e., hypothesis, H_1) in the CUT if its content X_0 exceeds the adaptive threshold, T. The null hypothesis, H_0 denotes the absence of the target in the CUT. From a finite sequence (i.e., CG-LNT clutter amplitudes) of clutter profile, $x_1, \dots, x_M$, the threshold T is calculated as a function of the estimated clutter level $\langle X \rangle$ and the predetermined scale factor τ. The latter controls the desired false alarm probability, Pfa. When the clutter parameter σ is known *a priori*, logt- OS-, WH-WHOS- and WHWH-CFAR procedures are used as shown in Figure. 3. 1 [28-33]. For the case of OS-, WH-, WHOS- and WHWH-CFAR detectors, the samples $x_1, \dots, x_M$, are sorted

to obtain $X_{(1)} < X_{(2)}, \ \ldots < X_{(M)}$ where $X_{(.)}$ denotes the specific ranked statistic of order *i, j, k* or *l*.

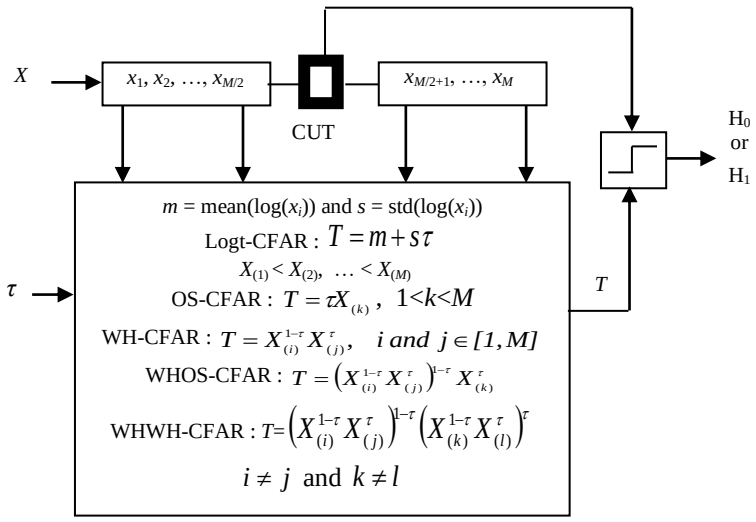

Figure. 3. 1 Existing CFAR detectors in CG-LNT clutter with known σ [28-33].

Note that, expressions of detection probability (Pd) and false alarm probability (Pfa) are difficult to obtain. In the presence of secondary targets, it is demonstrated that WH-CFAR, WHOS-CFAR and WHWH-CFAR algorithms are CFAR for Pareto type I, Weibull and log-normal distributed clutter with unknown parameters [30-33].

For the case of CG-LNT clutter, we select the two functions *g*(.) and *h*(.) as

$$\begin{cases} g(x_1, x_2, ..., x_M) = \left(X_{(i)}^{1-\tau} X_{(j)}^{\tau}\right)^{1-\tau} \left(X_{(k)}^{1-\tau} X_{(l)}^{\tau}\right)^{\tau} \\ h(x_1, x_2, ..., x_M) = X_{(m)} \end{cases} \tag{3.2}$$

Where *i, j, k, l* and *m* are integer numbers between 1 and *M* (i.e., € [1 *M*][5]).

Substituting (3.2) into (3.1), (3.1) becomes

$$X_0 \underset{H_0}{\overset{H_1}{\gtrless}} \left(X_{(i)}^{1-\tau} X_{(j)}^{\tau}\right)^{1-\tau} \left(X_{(k)}^{1-\tau} X_{(l)}^{\tau}\right)^{\tau} e^{\tau \log\left(\frac{X_{(m)}}{\left(X_{(i)}^{1-\tau} X_{(j)}^{\tau}\right)^{1-\tau}\left(X_{(k)}^{1-\tau} X_{(l)}^{\tau}\right)^{\tau}}\right)} \tag{3.3}$$

Simplifying (3.3), we obtain

$$X_0 \underset{H_0}{\overset{H_1}{\gtrless}} \left(\left(X_{(i)}^{1-\tau} X_{(j)}^{\tau}\right)^{1-\tau} \left(X_{(k)}^{1-\tau} X_{(l)}^{\tau}\right)^{\tau}\right)^{1-\tau} X_{(m)}^{\tau} \tag{3.4}$$

With the proviso that $i \neq j$ and $k \neq l$ so that (3.4) is meaningful.

This detector is labeled WHWHOS-CFAR procedure which is based on five order statistic, i.e., $X_{(i)}$, $X_{(j)}$, $X_{(k)}$, $X_{(l)}$ and $X_{(m)}$. Recall that the WHWHOS-CFAR detector is an extension of the existing WHWH-CFAR detector [31]. We will show below that this test uses five-order statistics in the presence of the two parameters CG-LNT clutter. After several tests, corresponding ranks of the ordered samples are calculated from simulated data giving a good estimation of the CG-LNT clutter levels. Table. 3. 1 shows the different test statistics of previous and proposed WHWHOS-CFAR detectors.

Table 3. 1 Possible CFAR test statistics obtained from (3.1)

CFAR algorithm	$g(.)$	$h(.)$	Threshold
CA-CFAR [27]	$\sum_{i=1}^{N} x_i$	1	$e^{\tau}\sum_{i=1}^{N} x_i \equiv \tau \sum_{i=1}^{N} x_i$
OS-CFAR [29]	$X_{(k)}$	1	$e^{\tau} X_{(k)} \equiv \tau X_{(k)}$
WH-CFAR [28]	$X_{(i)}$	$X_{(j)}$	$X_{(i)}^{1-\tau} X_{(j)}^{\tau}$
WHOS-CFAR [31]	$X_{(i)}^{1-\tau} X_{(j)}^{\tau}$	$X_{(k)}$	$\left(X_{(i)}^{1-\tau} X_{(j)}^{\tau}\right)^{1-\tau} X_{(k)}^{\tau}$
WHWH-CFAR [32]	$X_{(i)}^{1-\tau} X_{(j)}^{\tau}$	$X_{(k)}^{1-\tau} X_{(l)}^{\tau}$	$\left(X_{(i)}^{1-\tau} X_{(j)}^{\tau}\right)^{1-\tau}\left(X_{(k)}^{1-\tau} X_{(l)}^{\tau}\right)^{\tau}$
WHWHOS-CFAR (proposed)	$\left(X_{(i)}^{1-\tau} X_{(j)}^{\tau}\right)^{1-\tau}\left(X_{(k)}^{1-\tau} X_{(l)}^{\tau}\right)^{\tau}$	$X_{(m)}$	$\left(\left(X_{(i)}^{1-\tau} X_{(j)}^{\tau}\right)^{1-\tau}\left(X_{(k)}^{1-\tau} X_{(l)}^{\tau}\right)^{\tau}\right)^{1-\tau} X_{(m)}^{\tau}$

3. 3 Detection performance comparisons

In this Section, we investigate the performance of CFAR detectors discussed in Section 2 in presence of CG-LNT distributed clutter. Dependence of the Pfa against model parameters and the number of secondary targets is studied. In all simulations, the magnitude of target plus clutter is computed by

$$X = \sqrt{S^2 + C^2 + 2SC\cos(\varphi)} \tag{3.5}$$

Where S and C are respectively the target and clutter amplitudes and the random angle, $0<\varphi<2\pi$ has the uniform distribution. The clutter power is normalized to 1 (i.e., $E[X^2] = 1$ so that $\delta = exp\left(\sigma^2/2\right)^{-1}$). Below, CFAR properties and detection performances are presented using simulated and real IPIX (Intelligent PIxel X-band radar) data.

The McMaster IPIX radar sea clutter database is available with different sea and radar parameters [18]. The IPIX radar system is fully coherent X-band radar with dual transmit/receive antennas polarization, frequency agility and stare/surveillance mode. They are collected in Grimsby during winter 1998, on the shore of Lake Ontario. Graphical display of all 222 datasets and pictures including radar return plots and time Doppler spectra are available in [18]. Specifically, there are co-polarizations, HH and VV (Lpol), and cross-polarizations, HV and VH (Xpol), coherent reception, leading to a quadruplet of I and Q values for co-pol and cross-pol. Through the recordings, the radar was transmitting with a PRF of 1000 Hz and a pulse length of 0.06 us. The received IPIX data is treated by the arrival order and registered in a (60000x34) matrix where 34 denotes the number of range cells and 60000 is the number of pulses [18].

3. 3. 1 CFAR Properties Study

In this Subsection, the clutter environment is changed by CG-LNT clutter parameters (i.e., δ and σ) and the presence of interfering targets with an interfering-to-clutter ratio, ICR = 10dB. The size of the reference window is set to M = 32. The test statistics parameters, τ in (dB), i, j, k, l and m are determined with a desired Pfa value, 10^{-3} as shown in Table. 3. 2.

Table. 3. 2 Corresponding, parameters values found for each CFAR detector for M = 32 and Pfa =10^{-3}. '– ' denotes without using in T.

	Logt-CFAR	**OS-CFAR**	**WH-CFAR**	**WHOS-CFAR**	**WHWH-CFAR**	**WHWHOS-CFAR**
i	-	-	1	10	10	3
j	-	-	30	1	1	27
k	-	3M/4	-	27	5	22
l	-	-	-	-	27	17
m	-	-	-	-	-	5
τ	5.001	9.500	1.855	2.040	1.330	3.435

In order to verify CFAR properties of logt-, OS-, WHOS-, WHWH- and WHWHOS-CFAR detectors with equal range cells, a series of Pfa curves as a function of the scale factor τ in dB are obtained for three values of CG-LNT clutter shape parameter; σ = 0.5 (very spiky clutter case), σ = 1.5 (spiky clutter case) and σ = 3 (almost Gaussian clutter case).

As depicted in Figures. 3. 2 - 3.7, simulated data reveal that the WHWOS-CFAR detector exhibits the best CFAR property, since all Pfa curves are almost overlapped. This is due to the use of five ranked cells instead of one, two, three or four order statistics (cases of standard CFAR procedure). In these illustrations, τ is calculated in dB for each detector with a desired value of, Pfa = 10^{-3} (see Table. 3. 2). For several values of $0.5 < \sigma < 3$, the same remarks are observed as above about the CFAR properties as shown in Figure. 3. 8 using synthetic and real IPIX data.

Now, we examine the effect of the presence of interfering targets on the CFAR properties of underling CFAR detectors. In the presence of one and two secondary targets with ICR = 10dB in the reference window, it is clearly seen in Figures. 3. 9 and 3. 10 that the proposed CFAR detector keeps the best CFAR property for most values of σ.

Validation of our CFAR detector is investigated using available six recorded files of IPIX real data; i.e., file 1 with HH antennas polarization and 3m range resolution cell, file 2 (VV, 3m), file 3 (HH, 15m), file 4 (VV, 15m), file 5 (HH, 30m) and file 6 (VV, 30m). It is remarkable that WHWHOS-CFAR detector maintains the CFAR properties compared to classical CFAR detectors as depicted in Figures. 3. 11-3. 17. It is confirmed that, the proposed detector can be used in maritime surveillance radar with a minimum number of false alarms.

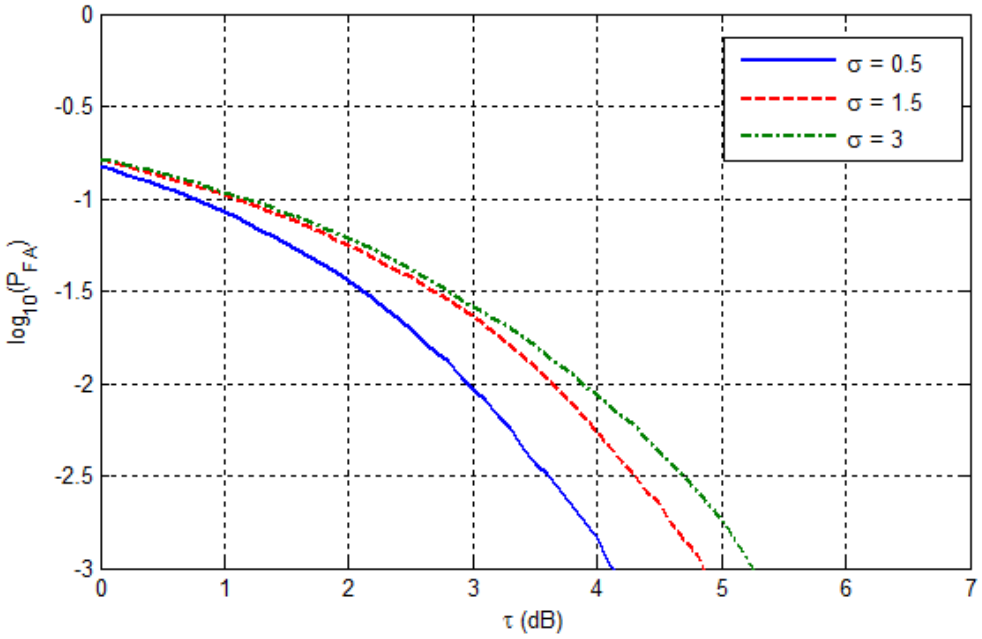

Figure. 3. 2 Illustration of CFAR property of logt-CFAR detector in CG-LNT sea-clutter with M = 32 and $\delta = exp\left(\sigma^2/2\right)^{-1}$.

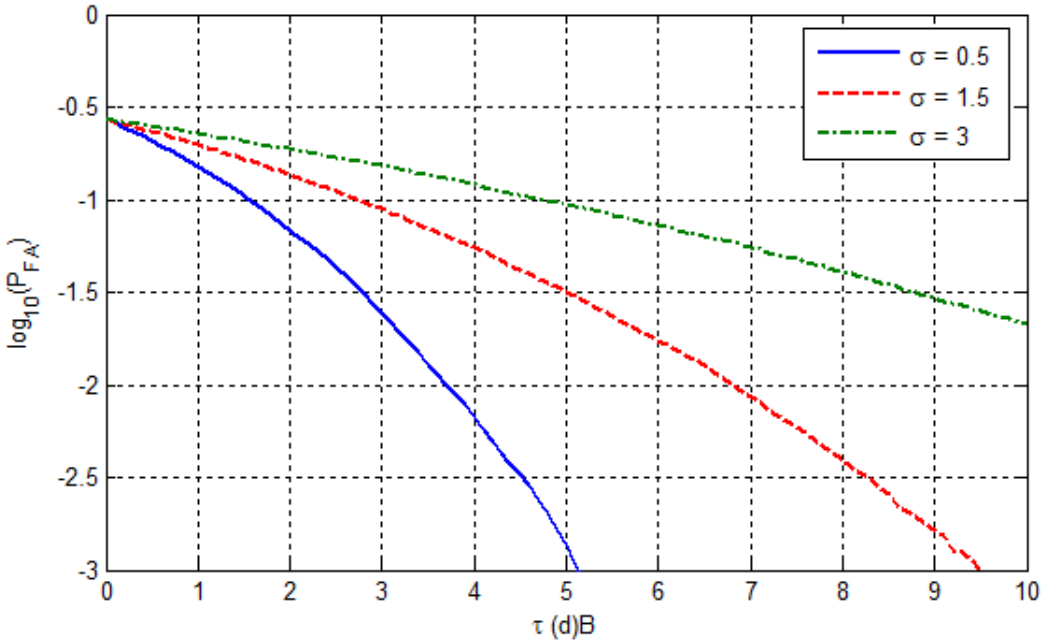

Figure. 3. 3 Illustration of CFAR property of OS-CFAR detector in CG-LNT sea-clutter with M = 32 and $\delta = exp\left(\sigma^2/2\right)^{-1}$.

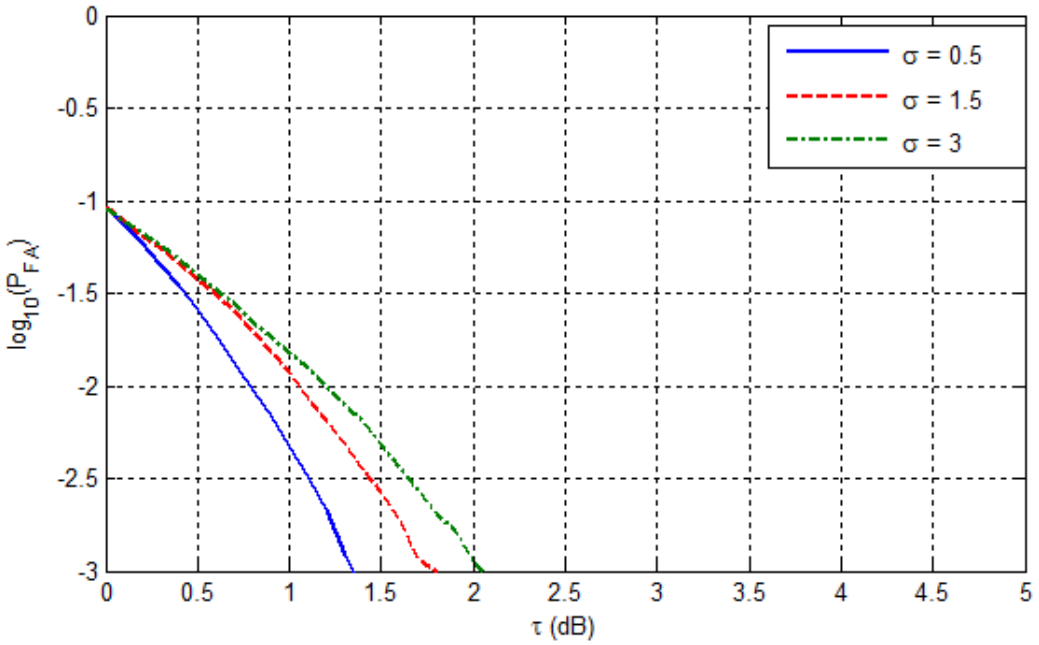

Figure. 3. 4 Illustration of CFAR property of WH-CFAR detector in CG-LNT sea-clutter with M = 32 and $\delta = exp\left(\sigma^2/2\right)^{-1}$.

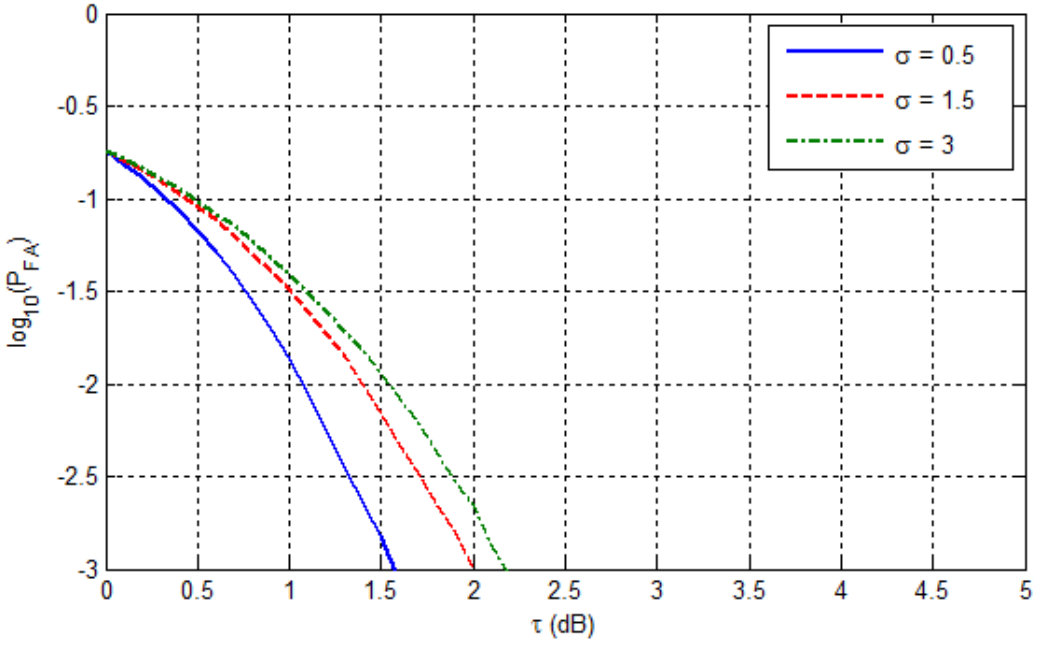

Figure. 3. 5 Illustration of CFAR property of WHOS-CFAR detector in CG-LNT sea-clutter with M = 32 and $\delta = exp\left(\sigma^2/2\right)^{-1}$.

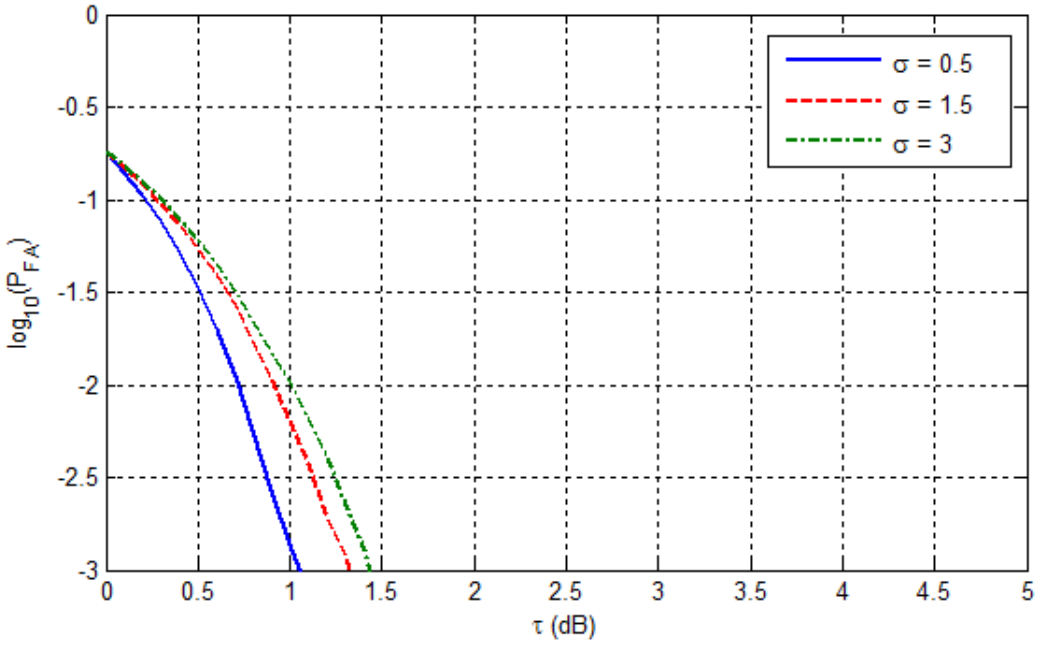

Figure. 3. 6 Illustration of CFAR property of WHWH-CFAR detector in CG-LNT sea-clutter with M = 32 and $\delta = exp\left(\sigma^2/2\right)^{-1}$.

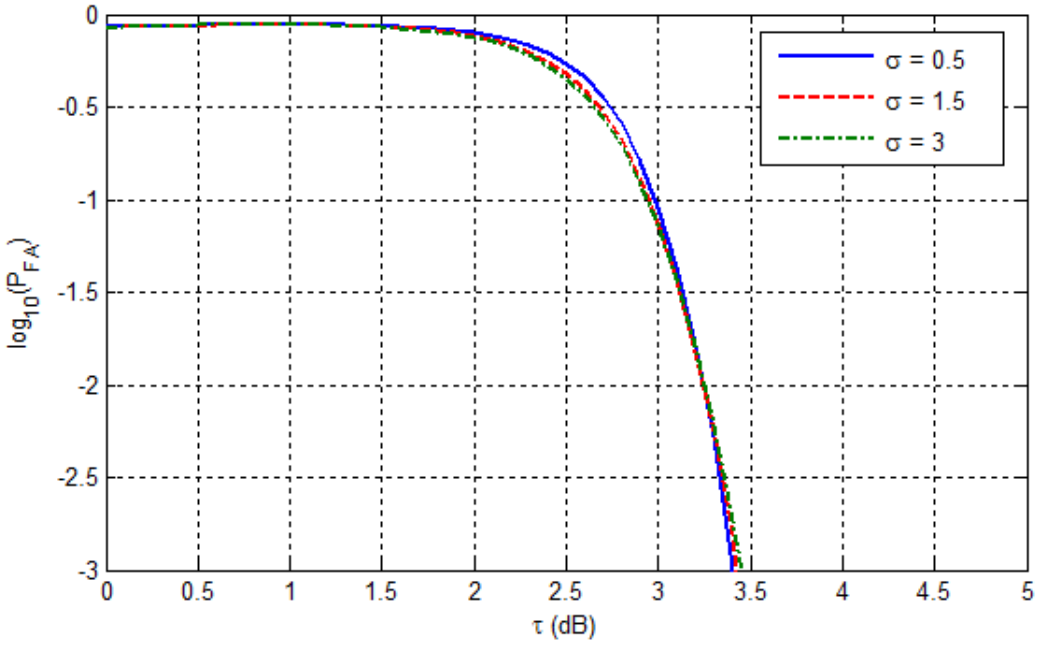

Figure. 3. 7 Illustration of CFAR property of WHWHOS-CFAR detector in CG-LNT sea-clutter with M = 32 and $\delta = exp\left(\sigma^2/2\right)^{-1}$.

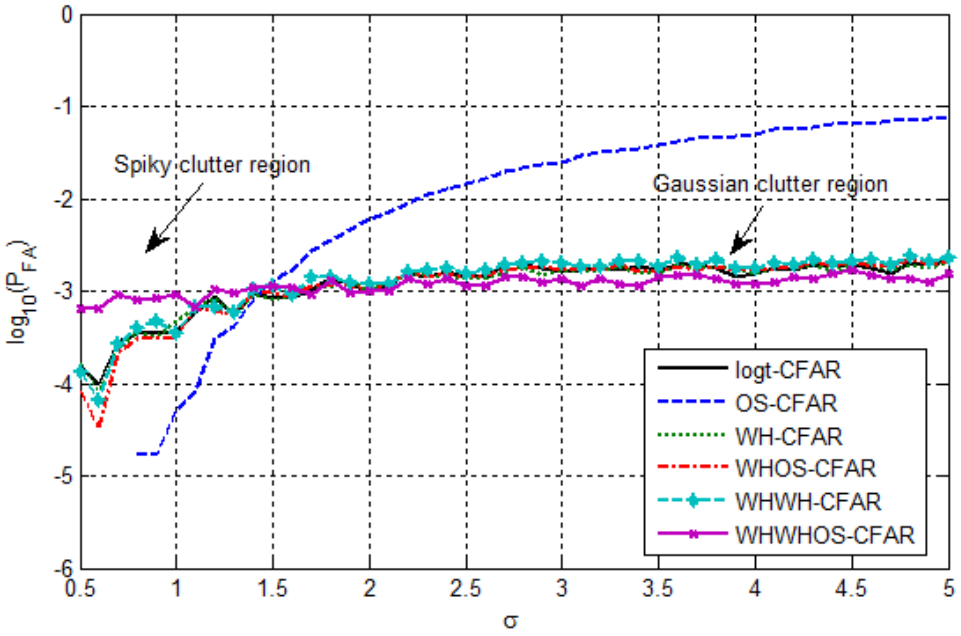

Figure. 3. 8 CFAR properties study of different CFAR detectors in terms of σ with M = 32 and $\delta = exp\left(\sigma^2/2\right)^{-1}$.

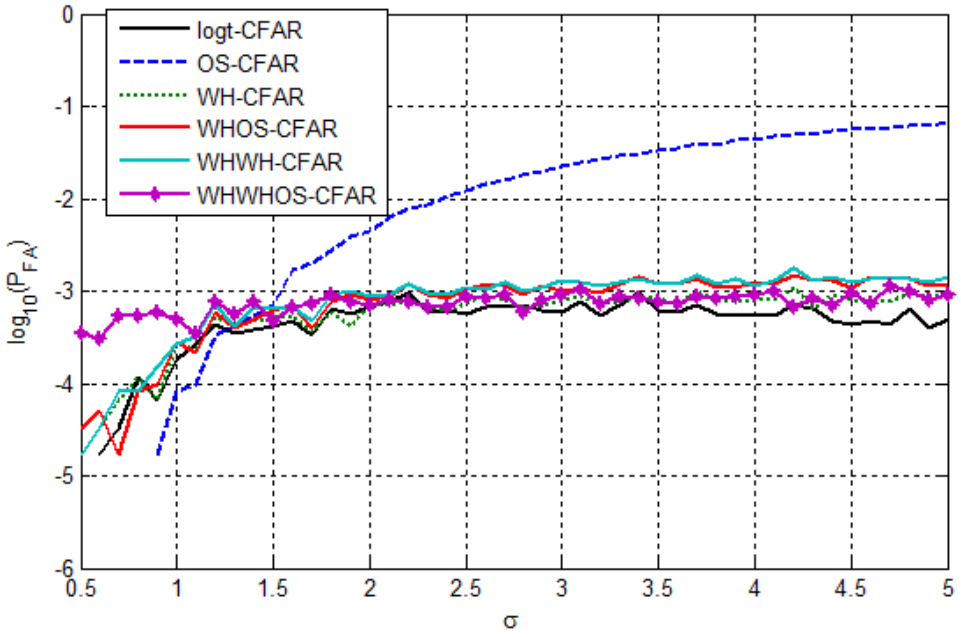

Figure. 3. 9 CFAR properties study of different CFAR detectors in terms of σ with 1 interfering target (ICR = 10 dB), M = 32 and $\delta = exp\left(\sigma^2/2\right)^{-1}$.

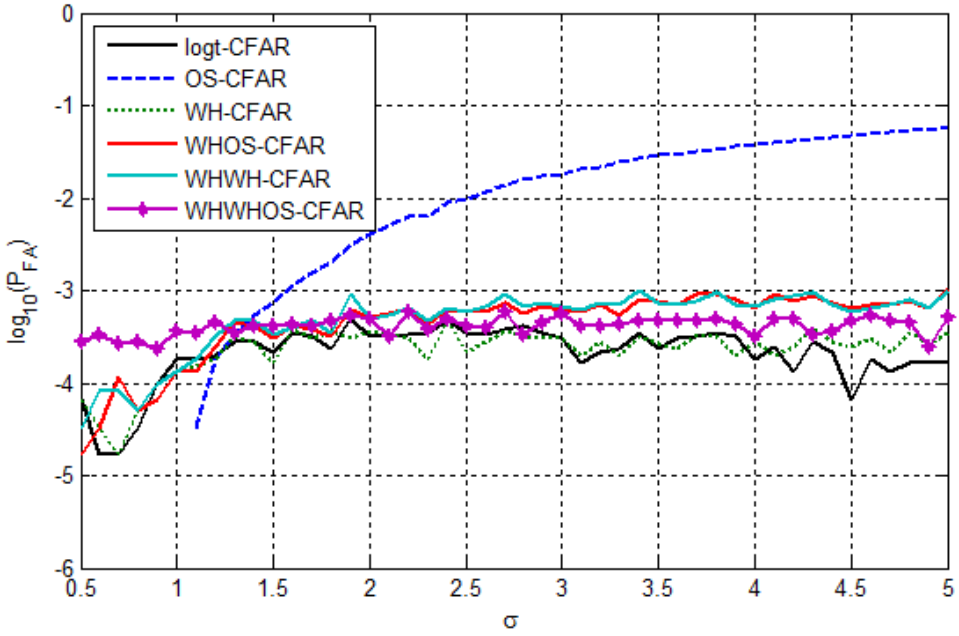

Figure. 3. 10 CFAR properties study of different CFAR detectors in terms of σ with 2 interfering targets (ICR = 10 dB), M = 32 and $\delta = exp\left(\sigma^2/2\right)^{-1}$.

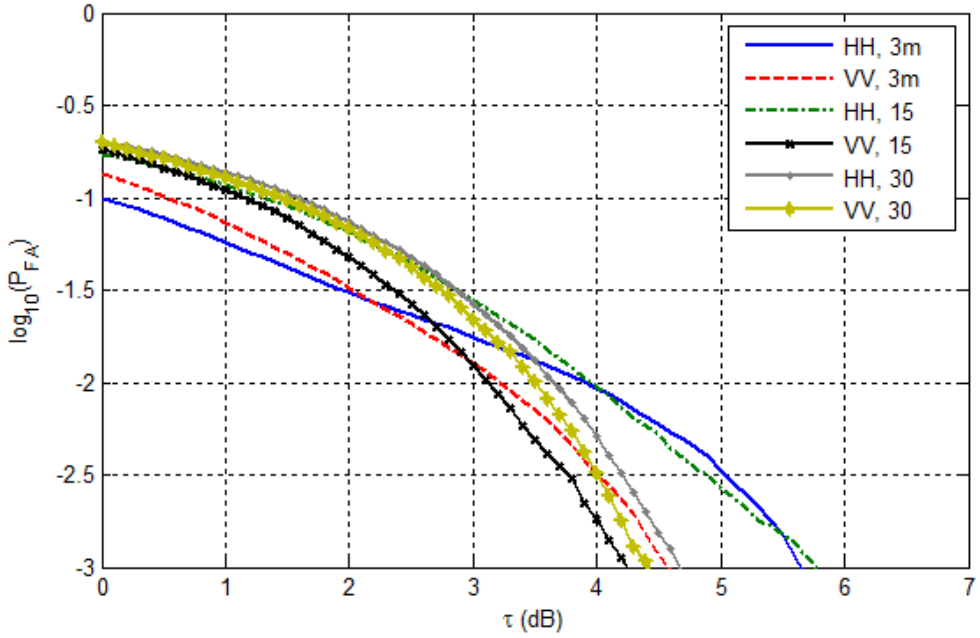

Figure. 3. 11 CFAR property of logt-CFAR detector in CG-LNT sea-clutter using real IPIX data.

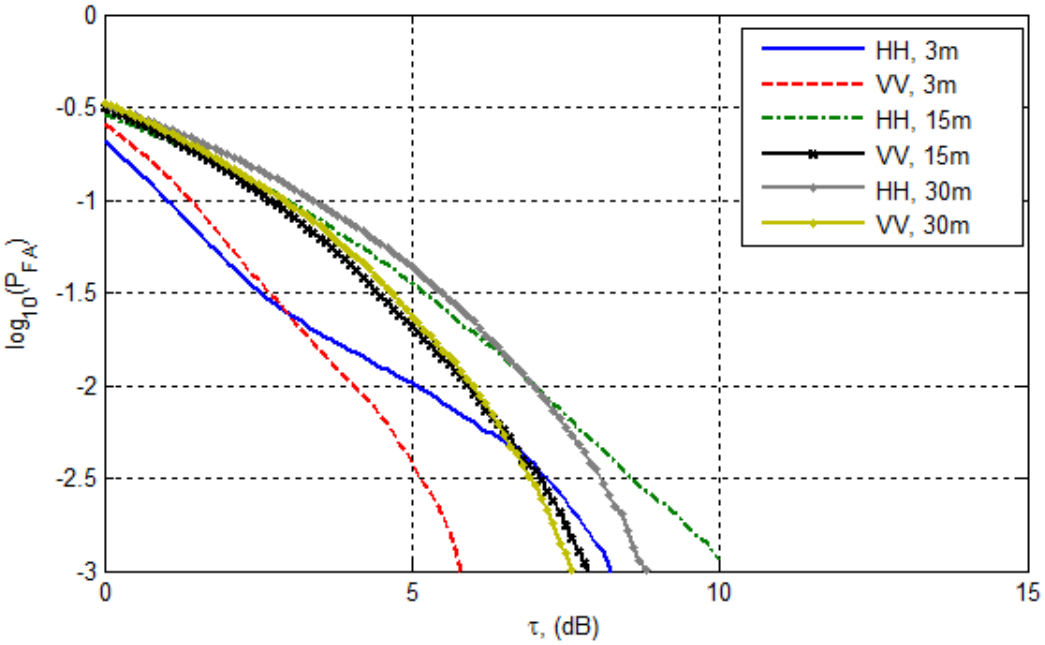

Figure. 3. 12 CFAR property of OS-CFAR-CFAR detector in CG-LNT sea-clutter using real IPIX data.

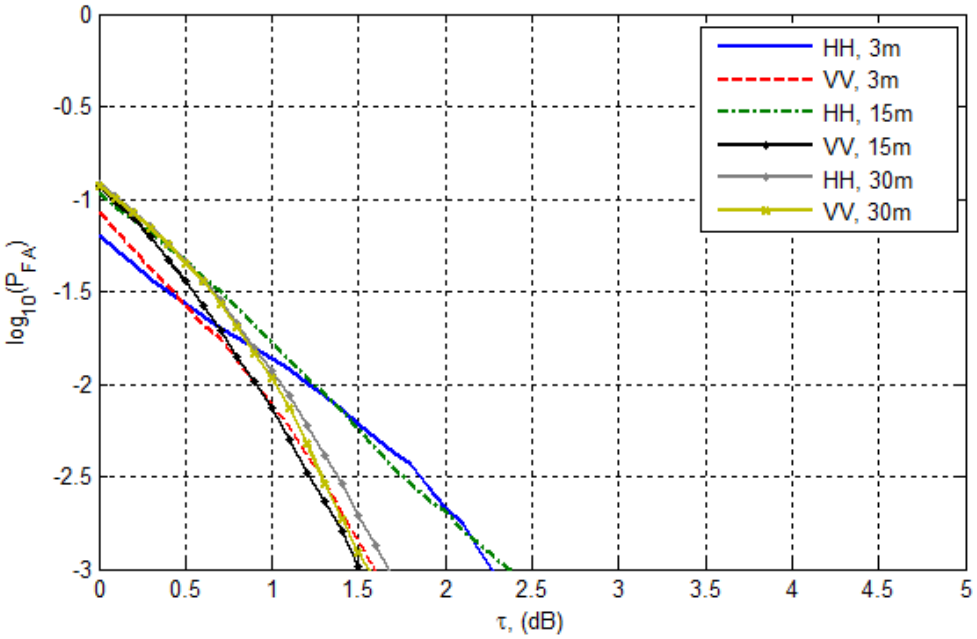

Figure. 3. 13 CFAR property of WH-CFAR-CFAR detector in CG-LNT sea-clutter using real IPIX data.

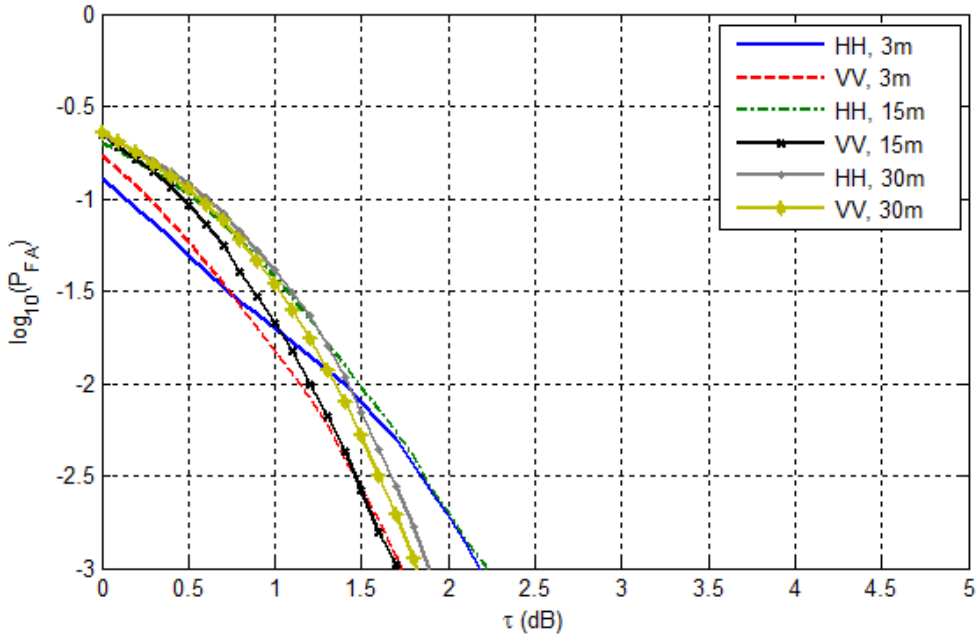

Figure. 3. 14 CFAR property of WHOS-CFAR-CFAR detector in CG-LNT sea-clutter Using real IPIX data.

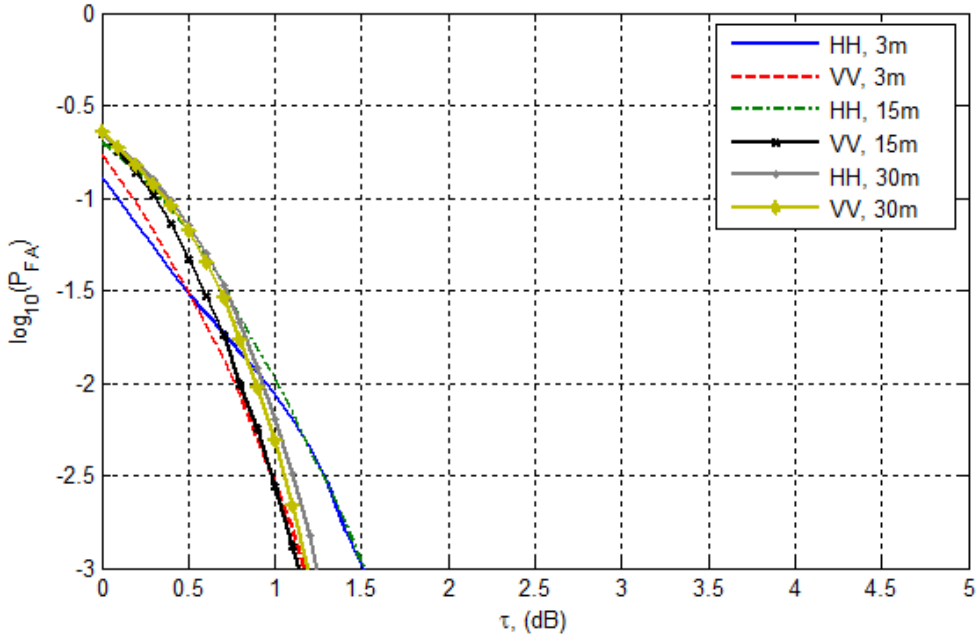

Figure. 3. 15 CFAR property of WHWH-CFAR-CFAR detector in CG-LNT sea-clutter using real IPIX data.

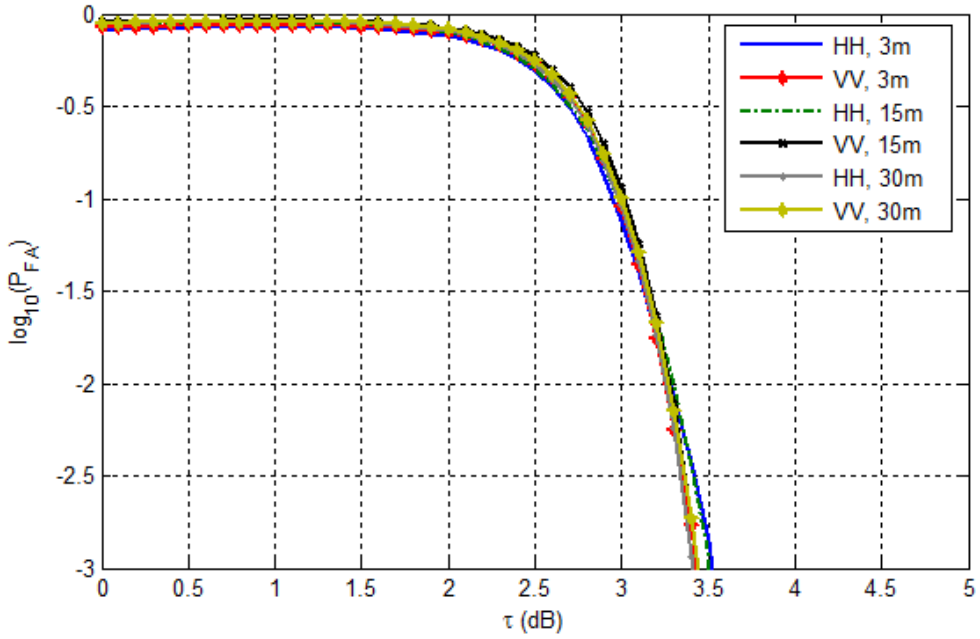

Figure. 3. 16 CFAR property of WHWHOS-CFAR-CFAR detector in CG-LNT sea-clutter using real IPIX data.

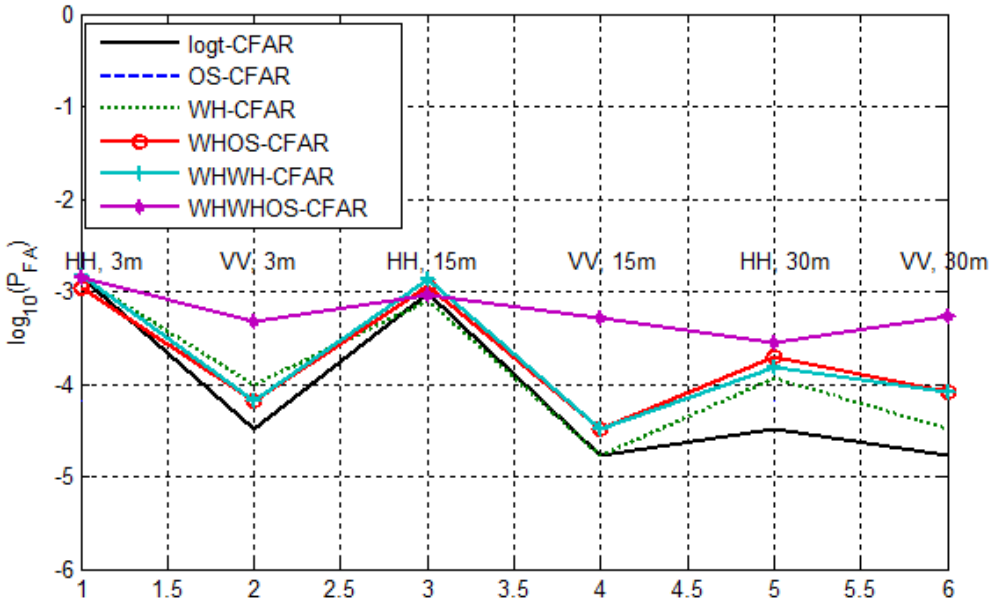

Figure. 3. 17 CFAR properties study of different CFAR detectors in terms of σ, M = 32 and $\delta = exp\left(\sigma^2/2\right)^{-1}$.

3. 3. 2 Detection Performances

In this Subsection, we consider the same parameters used in Subsection 3. 3. 1 for detection of Swerling I targets. The probabilities of detection as a function of signal-to-clutter ratio (SCR) are presented in Figures. 3. 18 – 3. 21.

In the absence or the presence of interfering targets, it is noticed that our CFAR detector has remarkable CFAR losses with respect to previous logt- OS-, WH-, WHOS- WHWH-CFAR algorithms as shown in Figures. 3. 18 – 3. 21.

If real data are used, the WHWHOS-CFAR is useful, because other CFAR detectors do not operate well in this spiky region of clutter, sine their CFAR properties are not acceptable. Similar observations as before are obtained, if we inject secondary targets in the reference window as depicted in Figures. 22 - 24.

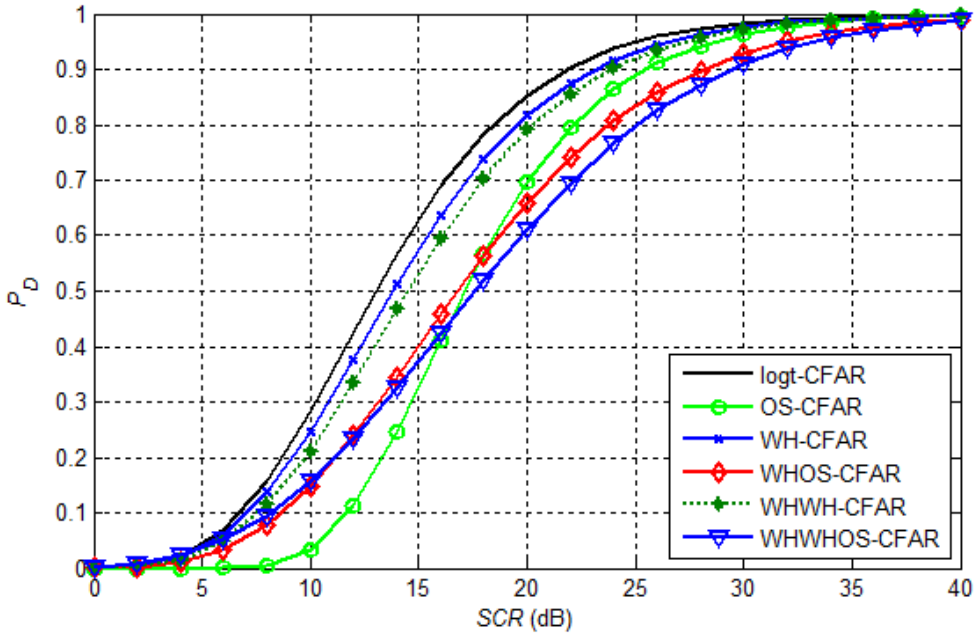

Figure. 3. 18 Detection probability of CFAR algorithms as a function of SCR for $M = 32$, $\sigma = 0.5$ and $\delta = exp\left(\sigma^2 / 2\right)^{-1}$.

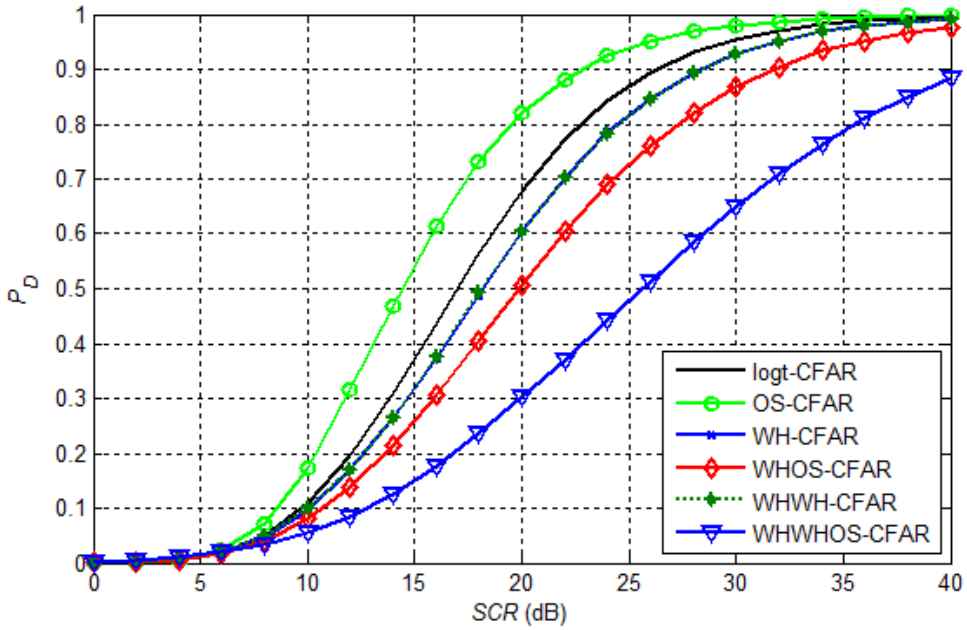

Figure. 3. 19 Detection probability of CFAR algorithms as a function of SCR for M = 32, σ = 1.5 and $\delta = exp\left(\sigma^2/2\right)^{-1}$.

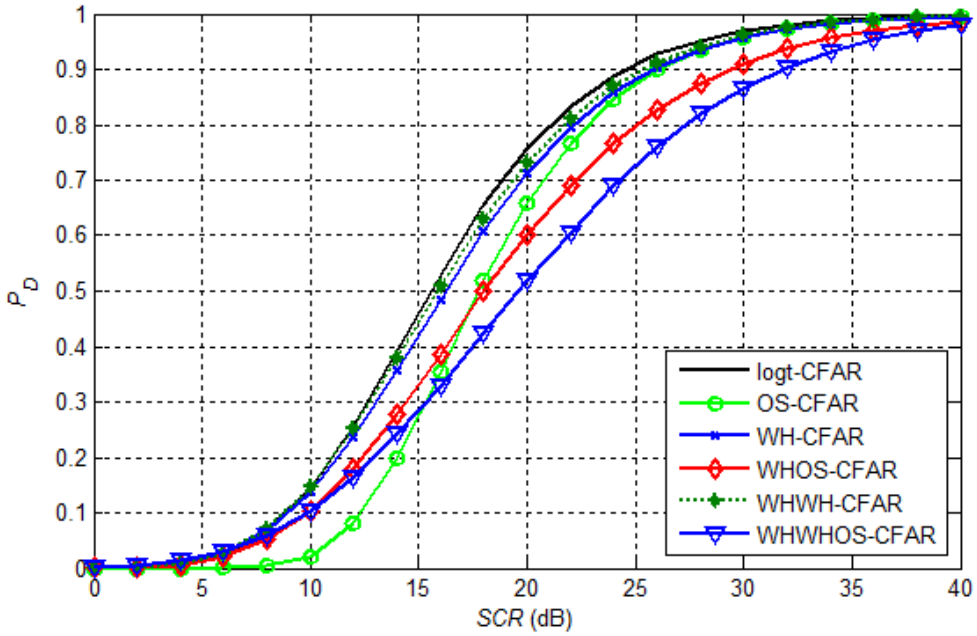

Figure. 3. 20 Detection probability of CFAR algorithms as a function of SCR for 1 interfering target, M = 32, σ =0.5 and $\delta = exp\left(\sigma^2/2\right)^{-1}$.

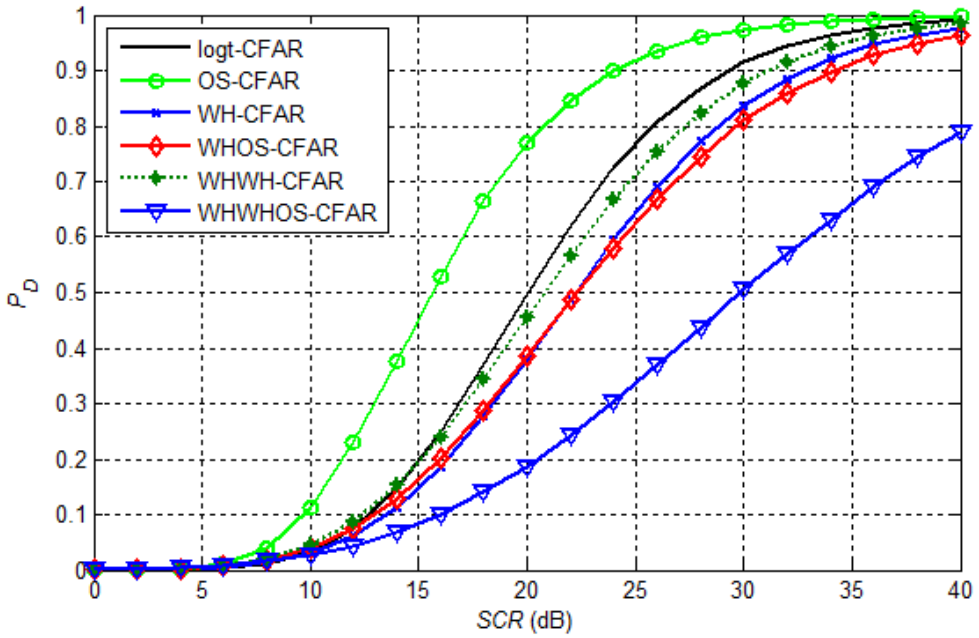

Figure. 3. 21 Detection probability of CFAR algorithms as a function of SCR for 2 interfering targets, M = 32, σ =1.5 and $\delta = exp\left(\sigma^2/2\right)^{-1}$.

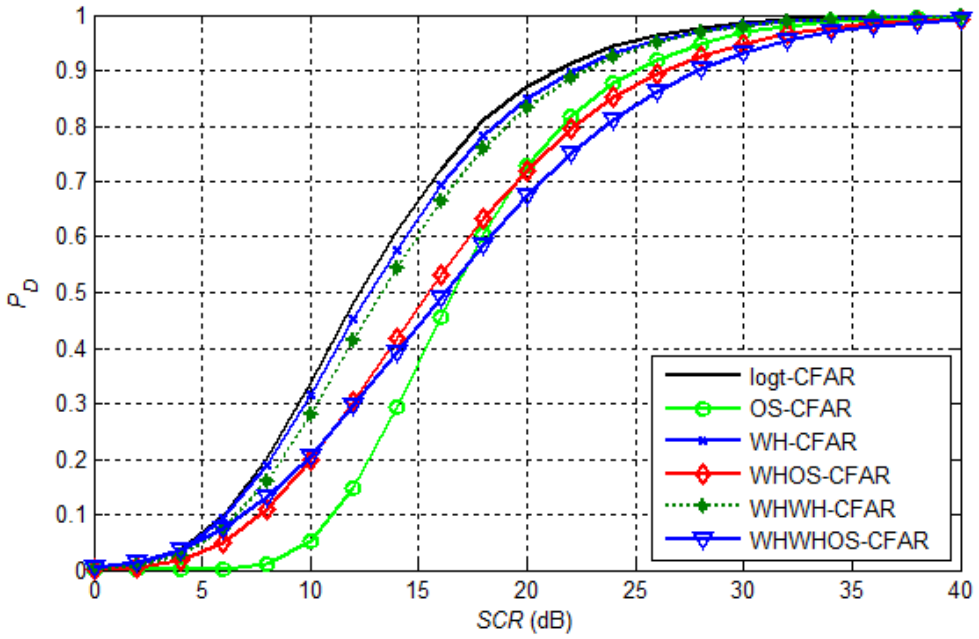

Figure. 3. 22 Detection probability of CFAR algorithms as a function of SCR using real data for M = 32, HH polarization and resolution 3m.

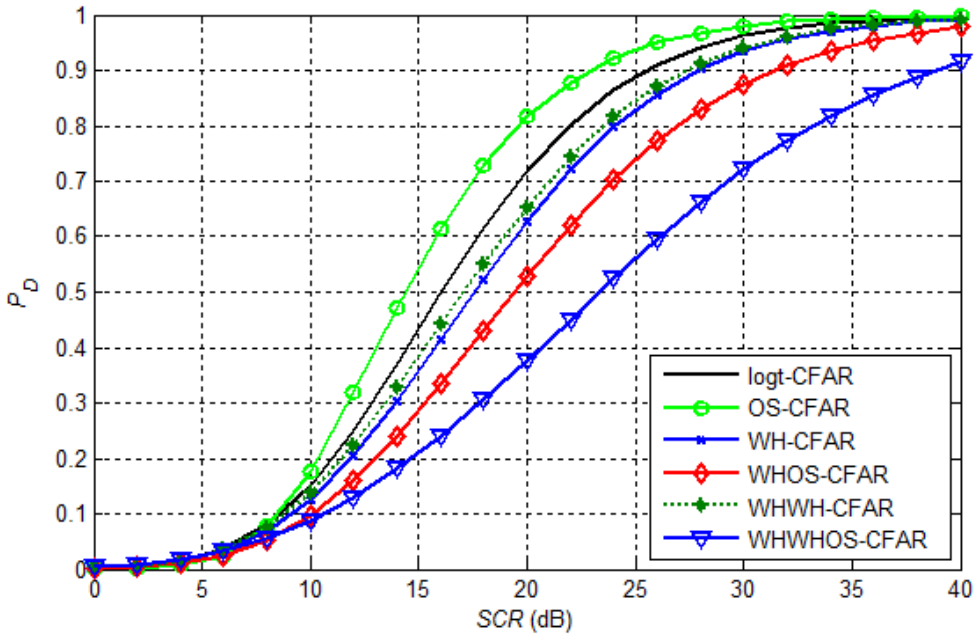

Figure. 3. 23 Detection probability of CFAR algorithms as a function of SCR using real data for 1 interfering target, M = 32, HH polarization and resolution 3m.

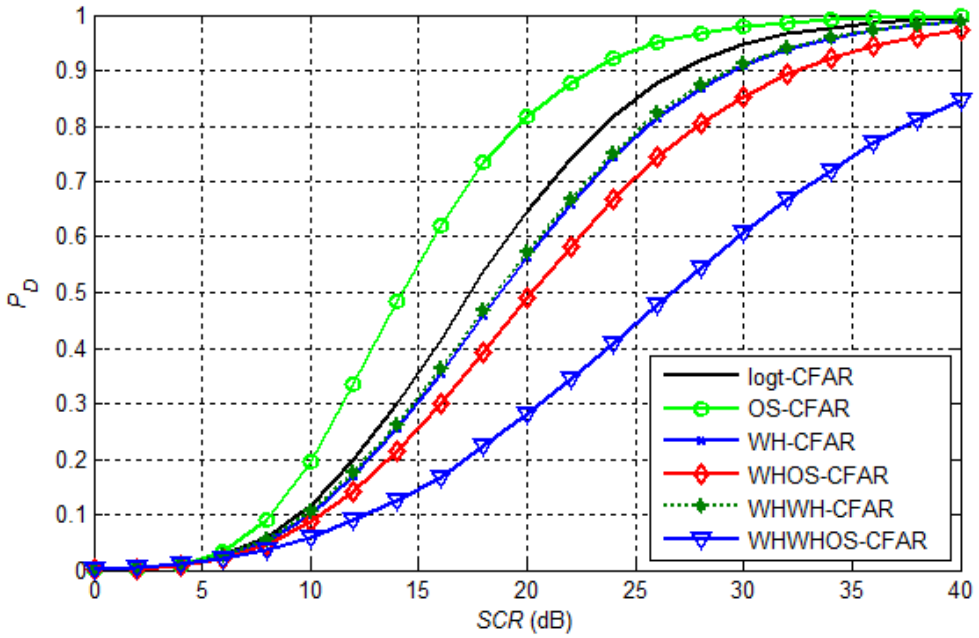

Figure. 3. 24 Detection probability of CFAR algorithms as a function of SCR

using real data for 2 interfering targets, $M = 32$, HH polarization and resolution 3m.

3. 4 Conclusion

In this Chapter, we focus on CFAR detection of Swerling I targets in the absence or the presence of secondary targets. First, CG-LNT distributed sea clutter is selected in this context as a correct description characteristic. Next, based on the general test statistic, two non-negatives invariants functions were selected and the proposed WHWHOS-CFAR was derived. Existing CFAR detectors were given for comparison purposes. Using conventional detectors, it has been seen from simulated results that the false alarm probability depends on the shape parameter in very spiky region. In this situation, the WHWHOS-CFAR detector almost maintains the desired constant false alarm probability for both simulated and real IPIX databases. However, CFAR losses of the proposed detector were greater than those obtained by existing CFAR algorithms for a single value of the standard deviation parameter.

General Conclusion

In this thesis, a new sea-clutter model labeled Trimodal generalized gamma population were suggested and examined over time diversity transmission. This theoretical model offers cumulative distributed function curves with a number of inflexion points. Really, this can fit numerous scenarios of IPIX database that cover in general a mixture of Rayleigh and non-Rayleigh clutter. Modeling comparison purposes were conducted against existing *K*+noise, CG-LNT+noise, GG and a mixture of two GG. It was shown that the proposed model exhibits the best fitting to real IPIX data in most cases.

For the purpose of improvements in detection performances particularly the CFAR properties, existing OS-CFAR and WHWH-CFAR algorithms were combined by means of the use of available general test statistic. This operation produces the proposed WHWHOS-CFAR maintaining a good CFAR property in presence of spiky clutter situations. The clutter was assumed to be CG-LNT without thermal noise with unknown scale and shape parameters. Through simulated and IPIX real data, the results of the derived WHWHOS-CFAR detector were compared providing low CFAR losses with respect to the above CFAR procedures.

The following paragraphs highlight main contents of presented chapters in this thesis:

In Chapter 1, we reviewed firstly the history of radar systems and their evolution over time, beginning with military uses and then transitioning to civilian applications such as weather monitoring, air traffic control, and maritime surveillance. The basic components of radar systems, such as the transmitter, receiver, and antenna, are explained, and how they operate by transmitting radio waves and receiving reflections to determine distance, speed, and direction were presented. Radar equations, classification concepts, and various applications were also discussed. Clutter and targets types were given by their probability density functions, including volume clutter, area clutter and Swerling targets.

In Chapter 2, Trimodal generalized gamma distribution were introduced as a correct description of sea reverberation data. The latter was given form a mixture of three GG distributions. For comparison purposes, classical distributions like *K*+noise, CG-LNT+noise and GG were considered after utilizing the NLSA estimation method for parameters finding of underling models. Experiments study showed that the Trimodal GG distribution is suitable for

modeling IPIX data in most cases. To demonstrate this, several scenarios of IPIX samples with different range resolutions and antennas polarizations were taken into account. The computational time associated with the proposed model is relatively high owing to the fact that they search eight dimensional spaces. To conclude, the application of the Trimodal GG distribution is a novel approach to modeling IPIX radar echoes. In fact, this model should produce excellent tail fitting of the other types of sea echoes.

In Chapter 3, we focused on CFAR detection of Swerling I targets in the absence or the presence of secondary targets. First, CG-LNT distributed sea clutter was selected in this context as a correct description characteristic. Next, based on the general test statistic, two non-negatives invariants functions were selected and the proposed WHWHOS-CFAR was derived. Existing CFAR detectors were given for comparison purposes. Using conventional detectors, it has been seen from simulated results that the false alarm probability depends on the shape parameter (standard deviation) in very spiky region. In this situation, the WHWHOS-CFAR detector almost maintains the desired constant false alarm probability for both simulated and real IPIX databases. However, CFAR losses of the proposed detector were greater than those obtained by existing CFAR algorithms.

Some suggestions of future research works are given below:

- Development of a new estimation approach for GG distributed parameters is essential using for instance the Deep learning technique.
- The WHWHOS-CFAR procedure can be applied for other distributions of sea clutter.

References

[1] C. Wolff, "*Les Principes du Radar*", Radartutorial.eu, July 11, 2021.

[2] L. Xingxing, X. Junhao, Z. Jie and F. L´evy, "A Flexible-Tailed Model for Radar Sea Clutter Amplitudes Based on the Smoothly Truncated", *IEEE Transactions on Aerospace and Electronic Systems*, Accepted, April 2, 2025.

[3] C. Zhaohui and Z. Min, "Reassigned bilinear transformation and Gaussian kernel function based approach for detecting weak target in sea clutter", *International Journal of Remote Sensing*, Vol. 37, no. 23, pp. 5668-5686, 2016.

[4] C. Wolff; "*Basic Principles of Radar*", Modified by Bill Murphy, Richardson RFPD, January 2012.

[5] H. Meikle, "*Modern Radar Systems*", 2nd Edition, Artech House, Boston, London, 2008.

[6] N. Levanon and E. Mozeson, "Radar Signals", John Wiley & Sons, Inc, 2004.

[7] M. Skolnik, "*Radar Handbook*", 3rd Edition, McGraw-Hill, 2008.

[8] Radar tutorial: Online available: https://www.radartutorial.eu

[9] M. R. Krattou, "Etude de la Détection Radar dans un Milieu Homogène", Magister thesis, University of Tlemcen, Department of Electronics, 2013.

[10] N. Boudaa and A. Helali, "Analyse des Processeurs CA-CFAR, OS-CFAR et OSGO-CFAR dans un Milieu Homogène et non Homogène", Master thesis, University of Blida 1, Department of Aircraft Construction, 2020.

[11] S. Chabbi, "Détection Adaptative CFAR à Censure Automatique Basse Sur Les Statistiques D'ordre En Milieux Non Gaussiens", Master thesis, University of Constantine, Département of Electronics, 2008.

[12] B. Rajeev, "Handbook of Engineering EM", 1st Edition, Marcel Dekker, 2004.

[13] Z. Terki, "Trimodal Discret Gamma Distribution and CFAR Detection with Multiple Pulses in Sea Clutter", Doctorate thesis, Department of Electronics and Communications, University of Ouargla, 2024.

[14] A. Mezache, Z. Terki and F. Chebbara, "Radar Clutter Modeling using CGIG and Mixture CGIG Distributions", *IEEE 5th Novel Intelligent and Leading Emerging Sciences Conference*, Nile University E gypt, pp. 21-23, 2023.

[15] A. Farina, F. Gini, M. V. Greco and L. Verrazzani, "High resolution sea clutter data: statistical analysis of recorded live data", *IEE Proceedings, Radar, Sonar & Navigation*, Vol. 144, no. 3, pp 121–130, 1997.

[16] Z. Terki, A. Mezache, F. Chebbara, "Modeling and parameter estimation of radar sea-clutter with trimodal gamma population", *Journal of Telecommunications and Information Technology*, no.2, pp. 82-90, 2022.

[17] S. Bocquet, L. Rosenberg and C. H. Gierull, "Parameter Estimation for a Compound Radar Clutter Model with Trimodal Discrete Texture", *IEEE Transactions on Geoscience and Remote Sensing*, Vol. 58, no. 10, pp. 7062 - 7073,2020.

[18] V. Anastassopoulos, G. A. Lampropoulos, A. Drosopoulos and M. Rey, "High Resolution Radar Clutter Statistics", *IEEE Transactions On Aerospace And Electronic Systems*. Vol. 35, no. 1, pp. 43 – 60, 1999.

[19] J. R. Nicholas, "Estimating the parameters of the K distribution in the intensity domain", *DSTO-TR-0839, Electronics and Surveillance Research Laboratory*, no. 011-015, pp. 1-76, 1999.

[20] I. Chalabi and A. Mezache, "Estimators of compound Gaussian clutter with log-normal Texture", *Remote Sensing Letters*, Vol. 10, no. 7, pp. 709–716, 2019.

[21] L. Rosenberg D.J. Crisp and N.J. Stacy, "Analysis of the KK distribution with medium grazing angle sea-clutter", *IET Radar, Sonar & Navigation*, Vol. 4, no. 2, pp. 209–222, 2010.

[22] Nelder-Mead algorithm: Online available: https://www.scilab.org/sites/default/files/neldermead.pdf

[23] McMaster IPIX Radar Sea Clutter Database: Online available: https://www.soma.crl.mcmaster.ca/ipix/

[24] A. Balleri, A. Nehorai and J. Wang, "Maximum likelihood estimation for compound-Gaussian clutter with inverse-gamma texture", *IEEE Transactions on Aerospace and Electronic Systems*, Vol. 43, no. 2, pp. 775—780, 2007.

[25] G. V. Weinberg, L. Bateman and P. Hayden, "Development of non coherent CFAR detection processes in Weibull background", *Digital Signal Processing*, Vol. 75, p. 96–106, 2018.

[26] K. Zebiri and A. Mezache, "Radar CFAR detection for multiple-targets situations for Weibull and log-normal distributed clutter ", *Signal, Image and Video Processing*, Vol. 15, no. 2, pp. 1671-1678, 2021.

[27] H. M. Finn and R. S. Johnson, "Adaptive detection model with threshold control as a function of spatially sampled clutter-level estimates", *RCA Review.*, Vol. 29, pp. 414-464, 1968.

[28] G. B. Goldstein, "False-alarm regulation in log- normal and Weibull clutter", *IEEE Transactions on Aerospace and Electronic Systems,* Vol. AES-9, no. 1, pp. 84–92, 1973.

[29] H. Rohling, "Radar CFAR thresholding in clutter and multiple target situations", *IEEE Transactions on Aerospace and Electronic Systems,* Vol. AES-19, no. 4, pp. 608-621, 1983.

[30] P. Weber and S. Haykin, "Ordered statistic CFAR processing for two-parameter distributions with variable Skewness", *IEEE Transactions on Aerospace and Electronic Systems*. Vol. 21, no. 6, pp. 819–821, 1985.

[31] K. Zebiri and A. Mezache, "Triple-order statistics-based CFAR detection for heterogeneous Pareto type I background", *Signal, Image and Video Processing*, Vol. 17, no. 4, pp. 1105-1111, 2022.

[32] K. Zebiri and A. Mezache, "Quadruple-order statistics CFAR algorithm for Pareto type I environment ", *Signal, Image and Video Processing*, Vol. 18, no. 3, pp. 2857-2863, 2024.

[33] K. Zebiri and A. Mezache, "CFAR detection using two scale invariant functions in heterogeneous Weibull clutter", *Signal, Image and Video Processing*, Vol. 18, no. 10, pp. 7285-7291, 2024.